論文 / 著書情報
Article / Book Information

題目(和文)	結晶およびアモルファスシリカの構造と熱挙動に関する分子動力学法による研究
Title(English)	Molecular dynamics study on structure and thermal behaviour of crystalline and amorphous silica
著者(和文)	山原圭二
Author(English)	
出典(和文)	学位:博士(理学), 学位授与機関:東京工業大学, 報告番号:乙第3571号, 授与年月日:2002年1月31日, 学位の種別:論文博士, 審査員:
Citation(English)	Degree:Doctor (Science), Conferring organization: Tokyo Institute of Technology, Report number:乙第3571号, Conferred date:2002/1/31, Degree Type:Thesis doctor, Examiner:
学位種別(和文)	博士論文
Type(English)	Doctoral Thesis

Molecular Dynamics Study on Structure and Thermal Behaviour of Crystalline and Amorphous Silica

Keiji Yamahara

2001

Contents

Abstract

Silica is one of the most important materials in the present electronics, optoelectronics, and chemical industries. It is a unique compound that has a variety of framework topologies, and shows complicated thermal behaviour such as displacive phase transitions and negative thermal expansion. In this study, the thermal behaviour of silica glass/melt, cristobalite, and an MFI-type zeolite was investigated from an atomistic viewpoint using MD simulations. The MD simulations qualitatively reproduce the displacive transitions of cristobalite and the MFI-type zeolite, and the negative thermal expansion of cristobalite and silica melt. Thus the MD simulations are widely effective not only for amorphous silica and known silica polymorphs but also for microporous crystals of zeolites. It is clarified that the thermal expansion of the crystalline silica is closely related to the distances between the nearest neighbor silicon atoms originating from the Si-O-Si bond angle. On the other hand, the thermal expansion of amorphous silica is dominated by longer-range structure such as network-forming rings. The MFI-type zeolite is predicted to exhibit a negative thermal expansion for the orthorhombic phase at higher temperatures, and to have a monoclinic *Pn* phase as well as the experimentally reported monoclinic $P2_1/n$ phase. Polymerization process yielding gels was also studied using MD simulations for silicic acid and monomethoxy silicic acid. The calculated Qn species distribution as a function of SiOSi/Si ratio is in good agreement with that observed by ^{1}H-NMR, suggesting the applicability of the MD simulations. A slow cluster growth during the early stage is followed by a rapid cluster growth due to cluster-cluster aggregation, and then the network structure become denser through the repeated bond-formation and bond-breaking resulting in phase separation. In addition, the remaining methoxy group interferes with the aggregation and the formation of the dense network structure.

Chapter 1

General Introduction

Silica and silicate minerals comprise 18 % and 96 % of the earth's crust, respectively [1]. Silica is thus the most abundant oxide on the earth's surface and then the familiar materials from ancient times. Table 1.1 lists the staple uses of silica today. Silica glass crucibles and tubes are used as containers for silicon crystal growth, diffusion doping and epitaxial growth processes on integrated circuit chips due to high-temperature stability. Optical glass fiber is used for the long-distance telecommunication because of excellent optical transmission. The high purity silica glass, thus, plays an important role in the present electronics and optoelectronics industries. On the other hand, zeolites, molecular level porous materials, are used as catalysts having high shape-selectivity for several types of chemical reaction i.e. cracking, isomerization and hydrocarbon synthesis. Those are also used as molecular sieves for gas separation. The advantage of zeolite catalysts and adsorbents would be controllability of their performance by choosing the type of zeolites or modifying the microporous structure by ion exchange, dealuminization etc.

Table 1.1 Industrial uses of silica.

Forms	Uses
Quartz	Quartz oscillator
Zeolite	Catalyst, molecular sieve, adsorbent
Glass	Otical fiber, IC photomask, semiconductor process ware (crucble, boat, tube), IC encapsulation material
Gel	Catalyst support, drying agent, chromatograph column

Silica has several known polymorphs (cristobalite, tridymite, quartz, coesite and stishovite), in addition to two classes of porous framework structures (zeolites and clathrates). It is easy to make amorphous silica (glass and gel). The phase diagram for the silica system is drawn in Fig. 1.1 [2]. The international zeolite association (IZA) has approved 98 framework topologies as unique zeolite structure comprising

silicates [3]. The extensive polymorphism of silica is closely related to the characteristics of Si-O bonding. Fig. 1.2 (upper) illustrates an SiO_4 tetrahedron that is a fundamental unit of the silica and silicate structures. In the silica structure, oxygen atoms at the corners are shared between two SiO_4 tetrahedra generating a three-dimensional network as shown in Fig. 1.2 (lower), with the exception of the high-pressure stishovite polymorph. Framework topology can be described by the size of rings comprising the tetrahedra, the composition of ring sizes, and the linkage pattern of the rings. The potential energy curve for Si-O-Si bond angle in bitetrahedron is obtained by *ab initio* calculation, as shown in Fig. 1.3 [4]. The energy curve is relatively flat at angles wider than the minimum energy angle, suggesting a variety of Si-O-Si angle, while it is steep at angles narrower than that. Consequently, the topological diversity of silica is closely related to the flexibility of the inter-tetraheral angle (Si-O-Si angle) as well as the corner-sharing tetrahedral network. The diverse framework topology and the flexibility of Si-O-Si angle may influence the thermal behaviour of silica.

Low-pressure crystalline phases, quartz, tridymite, and cristobalite, present displacive transitions, produced by small displacements of the silicon and oxygen atoms, conserving the tetrahedra connections but increasing the crystal symmetry upon heating above room temperature [5]. Furthermore, the high temperature phases of these three polymorphs also present nearly zero or slight negative thermal expansion. The thermal behaviour would be related to their open frameworks, which may provides space for displacements of framework atoms and enlargement in the motions of the atoms. In the application of silica materials, the effect of the thermal behaviour is of interest and practically important. Actually, the lattice dynamics of zeolite frameworks are suggested to influence the performance of zeolite materials in catalytic and sorptive applications. The pore window motion of zeolite frameworks has been studied using constant volume molecular dynamics (MD) simulation [6]. This simulation indicates that the definition, extent, and period of the motion depend on the framework topology.

Although an MFI-type zeolite, which is known to present displacive transition, is studied, the influence of the transition on the pore window motion could not be investigated. There are some static studies of the phase transition for the MFI-type zeolite using lattice energy minimization without the notice of the dynamics of the framework atoms [7,8]. Unfortunately, no MD study successfully followed the displacive transition of the MFI-type zeolite.

The physical and chemical properties of glass such as optical transmittance, chemical durability, viscosity, mechanical strength depend on the fictive temperature of glass. The fictive temperature (T_f) is defined as "the temperature at which the glass would find itself in equilibrium if suddenly brought to that temperature from its given state" [9]. The silica glass structure is expected to vary with T_f. In fact, the change in average Si-O-Si bond angle with T_f is demonstrated from X-ray analysis [10], and shifts in the bands of Raman [11] and infrared absorption spectra [12]. However, it has not been clarified how the local structural change affects long range structure and density. The density anomaly for silica melt is experimentally observed that the thermal expansion coefficient is negative in the temperature range from 1000 to 1550°C, and positive at higher temperatures [13]. Although the negative thermal expansion was connected to the negative thermal expansion of β-cristobalite, this has not been confirmed.

It is desirable that the mechanism of the complicated thermal behaviour for crystalline and amorphous silica is examined considering the influence of the framework topology. The knowledge obtained like that is generalized in the silica polymorphism, which is significant in the application of silica materials. MD simulation is very useful for that study, because the effect of network topology can be extracted ideally, as well as macroscopic quantities such as enthalpies and lattice constants are obtained with the motion of atoms as a function of time.

Another interest is in the structural formation process of silica, which takes various framework topologies. The deepening of the science of the formation process should

promote the development of new silica material. There are actually plenty of experimental reports in this field. Brinker and Scherer [14] present the physical and chemical principles of the sol-gel process under a coherent account by exploring the numerous data. The kinetics of hydrolysis and condensation reactions are analyzed using ^{1}H and ^{29}Si nuclear magnetic resonance spectoscopy (NMR), which can determine the nearest neighbor of Si i.e. an alkoxide group (OR), a hydroxyl group (OH), or a bridging oxygen (OSi). Infrared and Raman spectroscopy are used to identify specific oligomeric species in solution and to follow the polymerization of silicate frameworks in combination with NMR. Small-angle-scattering investigations elucidate the growth and topology of macromolecular networks that precede gelation, the aggregation of colloids, and the structure of gels. There is also enormous amount of work done to model aggregation processes, which leads to the kinetics of growth and the fractal structure of the resulting clusters. However, there is not sufficient work to simulate the growth of silicate frameworks on an atomic level, which incorporates the character of Si-O bonding. Garofalini and Martin [15] first applied MD simulations for the structural development of silica gel. Their results for silicic acid were consistent in the feature of growth process with experimental NMR data. For the real system, the influence of alcoxide group on structural development is considerable because hydrolysis and condensation reactions proceed concurrently. Further MD study is necessary on the growth process considering the effect of the alcoxide group.

In this study, the thermal behaviour of amorphous silica and silica polymorphs including the displacive phase transition and the negative thermal expansion is discussed from an atomistic viewpoint using MD simulations. The interatomic potential models employed are based on an empirical model developed by Kawamura to reproduce the structure and its pressure and temperature dependence for various silica crystals such as quartz, cristobalite, and stishovite [16]. The polymerization process yielding gel is also examined using MD simulation to extract the detailed picture of structural development considering the effect of methoxy group. For this simulation, the interatomic potential

model used is the same as that developed by Feuston and Garofalini [15] except an additional term for methoxy groups. The present study described in this thesis is divided into three parts as follows: (1) Thermal behaviour of silica glass/melt and cristobalite in Chapter 2, (2) thermal behaviour of an MFI-type of zeolite in Chapter 3, and (3) structural development in sol-gel process for silica in Chapter 4. MD simulation cells related to the study appear in Figs 1.4 –1.7.

References

[1] K.H. Wedephl, in: Geochemistry (Holt, Reinhart and Winston, New York) p.67.

[2] Peter J. Heaney, in: Silica, eds. P.J. Heaney, C.T. Prewitt and G.V. Gibbs (Mineralogical Society of America, Washington, 1994) p.2.

[3] Ch. Baerlocher, W.M. Meier and D.H. Olson, Atlas of zeolite framework types (Elsevier, 2001).

[4] M.D. Newton and G.V. Gibbs, Phys. Chem. Miner., 6 (1980) 221

[5] G. Dolino, in: Structure and Imperfections in Amorphous and Crystalline Silicon Dioxide, ed. R.A.B. Devine, J.-P. Duraud, and E. Dooryhee (John Wiley & Sons, 2000) p. 49.

[6] M.W. Deem, J.M. Newsam, and J.A. Creighton, J. Am. Chem. Soc., 114 (1992) 7198.

[7] R.G.Bell, R.A.Jackson, and C.R.A.Catlow, J. Chem. Soc., Chem. Commun, (1990) 782.

[8] E.de Vos Burchart, H.van Bekkum, and B.van de Graaf, Zeolites, **13** (1993) 212.

[9] A.Q. Tool, J. Am. Ceram. Soc. 29 (1946) 240.

[10] V.E. Sokol'ski, V.A. Shovskii, V.P. Kazimirov and G.I. Batalin, Soc. J. Glass phys. Chem. (Transl.) 6 (1980) 338.

[11] A.E. Geissberger and F.L. Galeener, Phys. Rev. B28 (1983) 3266.

[12] A. Agarwal, K.M. Davis, M. Tomozawa, J. Non-Crystaliine Solids, 185 (1995) 191.

[13] R. Brückner, J.Non-Cryst.Solids, 5 (1970) 123.

[14] C.J. Brinker and G.W. Scherer, Sol-Gel Science (Academic Press, San Diego, CA, 1990).

[15] S.H. Garofalini and G.E. Martin, J. Phys. Chem., 98 (1994) 1311.

[16] K. Kawamura, in: Molecular Dynamics Simulations, ed. F. Yonezawa (Springer-Verlag, Berlin, 1990) p. 88.

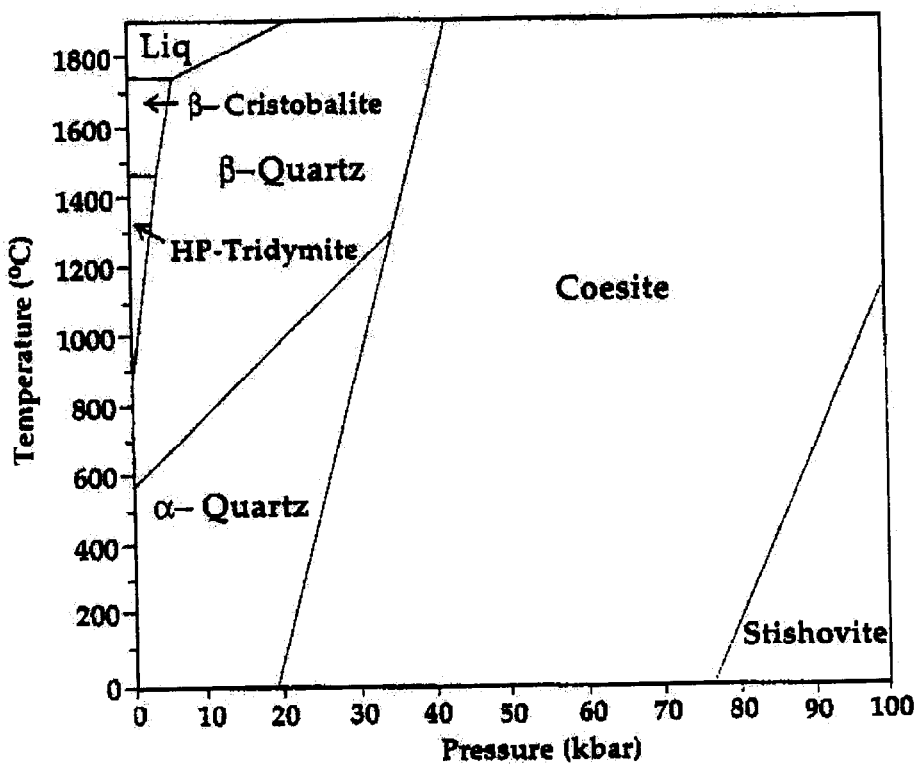

Fig. 1.1 Phase diagram for the silica system [2].

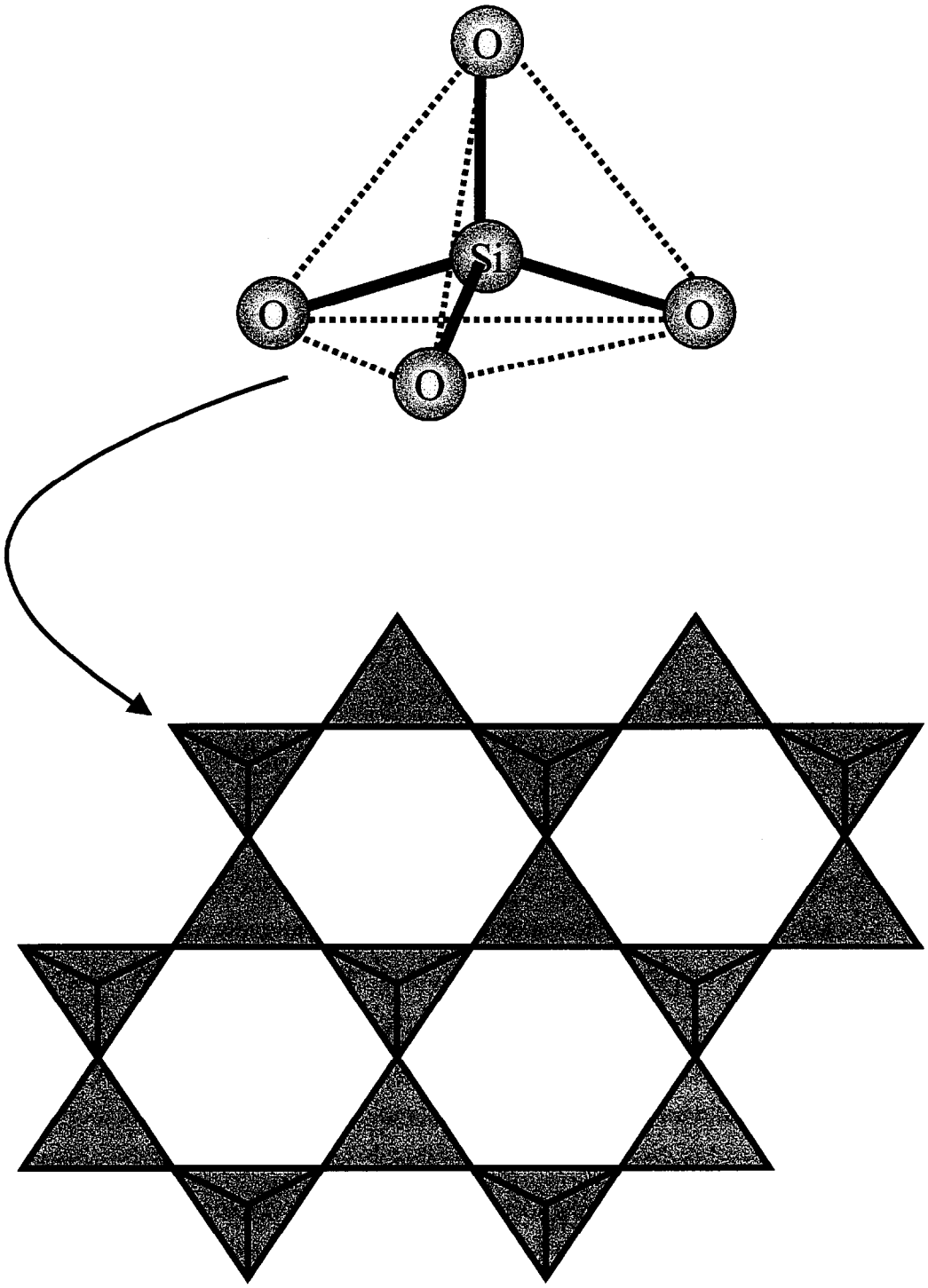

Fig. 1.2 SiO_4 unit (upper) and SiO_4 network (lower).

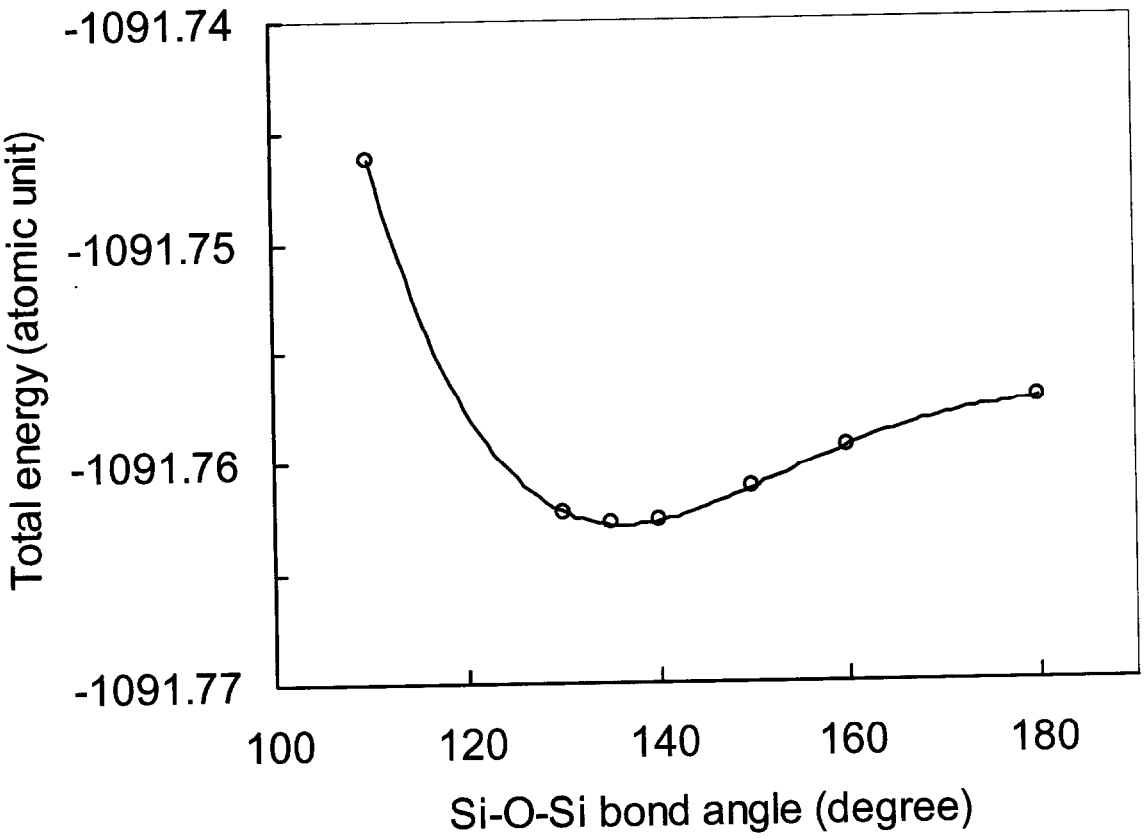

Fig. 1.3 Potential energy curve obtained by *ab initio* calculation as a function of the Si-O-Si angle in pyrosilicic acid molecule, $H_6Si_2O_7$ [4]. Si-O bond lengths are 1.62 Å. The minimum energy Si-O-Si angle is 137° .

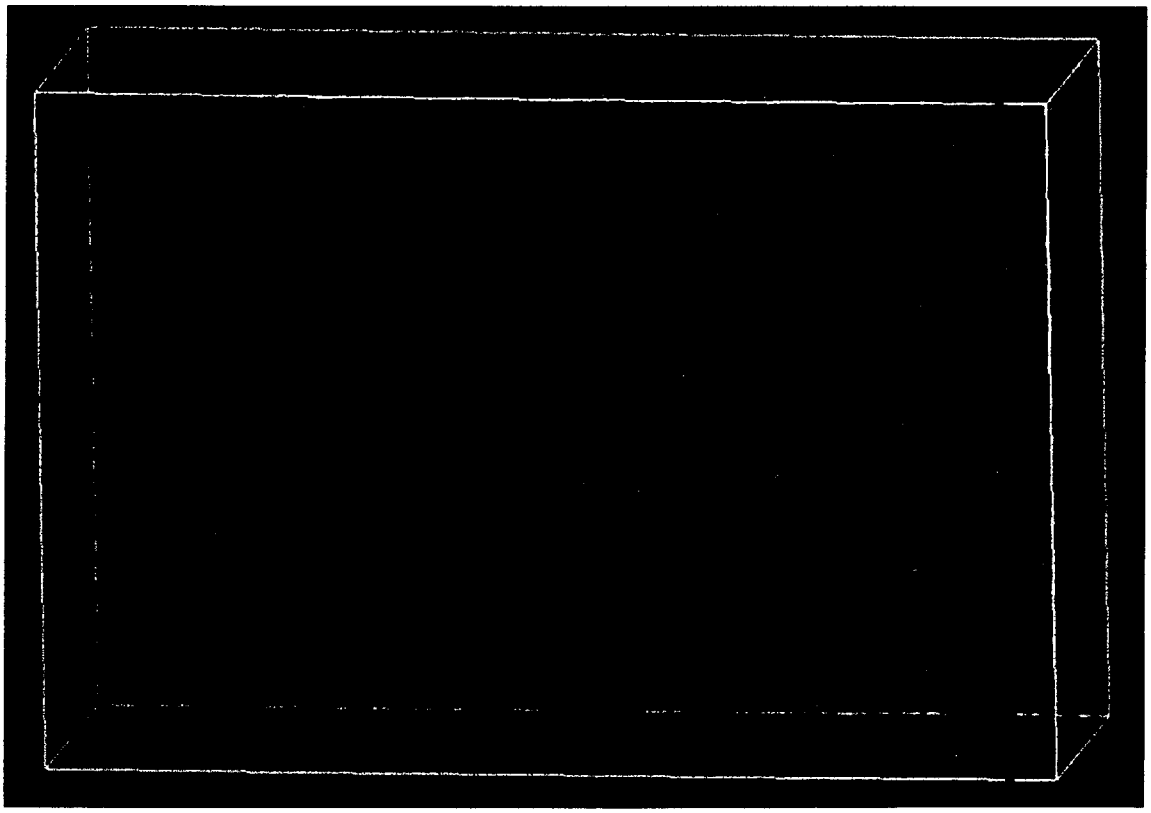

Fig. 1.4 An MD simulation cell for amorphous silica. The simulated system is composed of 3000 atoms (1000 Si and 2000 O). The cell shown is shortened to a quarter in depth. Yellow and red spheres represent silicon and oxygen atoms, respectively. White lines indicate a crystal unit cell.

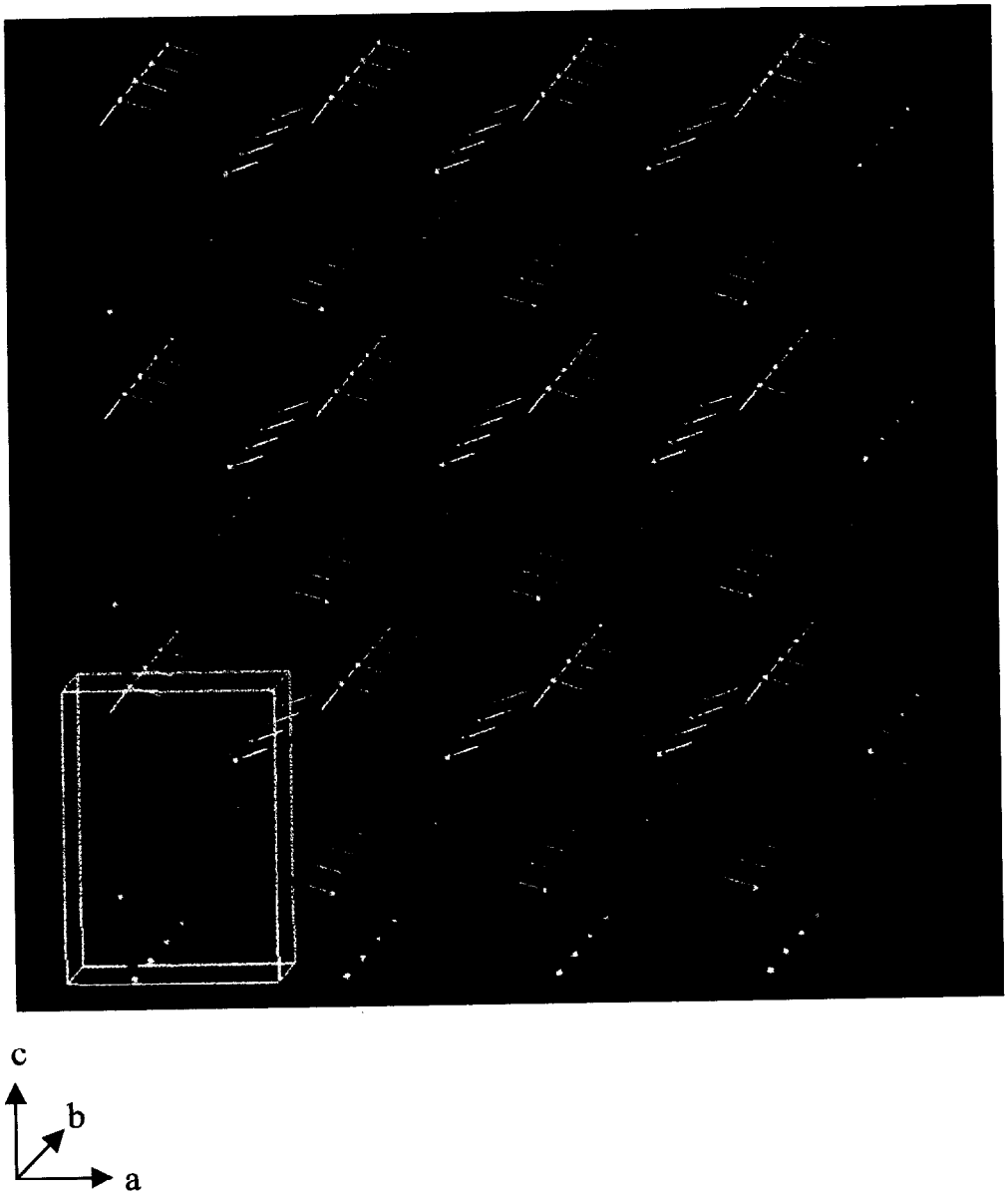

Fig. 1.5 An MD simulation system for α-cristobalite. The system is composed of 576 atoms (192 Si and 384 O), corresponding to an array of 4 × 4 × 3 crystal unit cells. Yellow and red spheres represent silicon and oxygen atoms, respectively. White lines indicate a crystal unit cell.

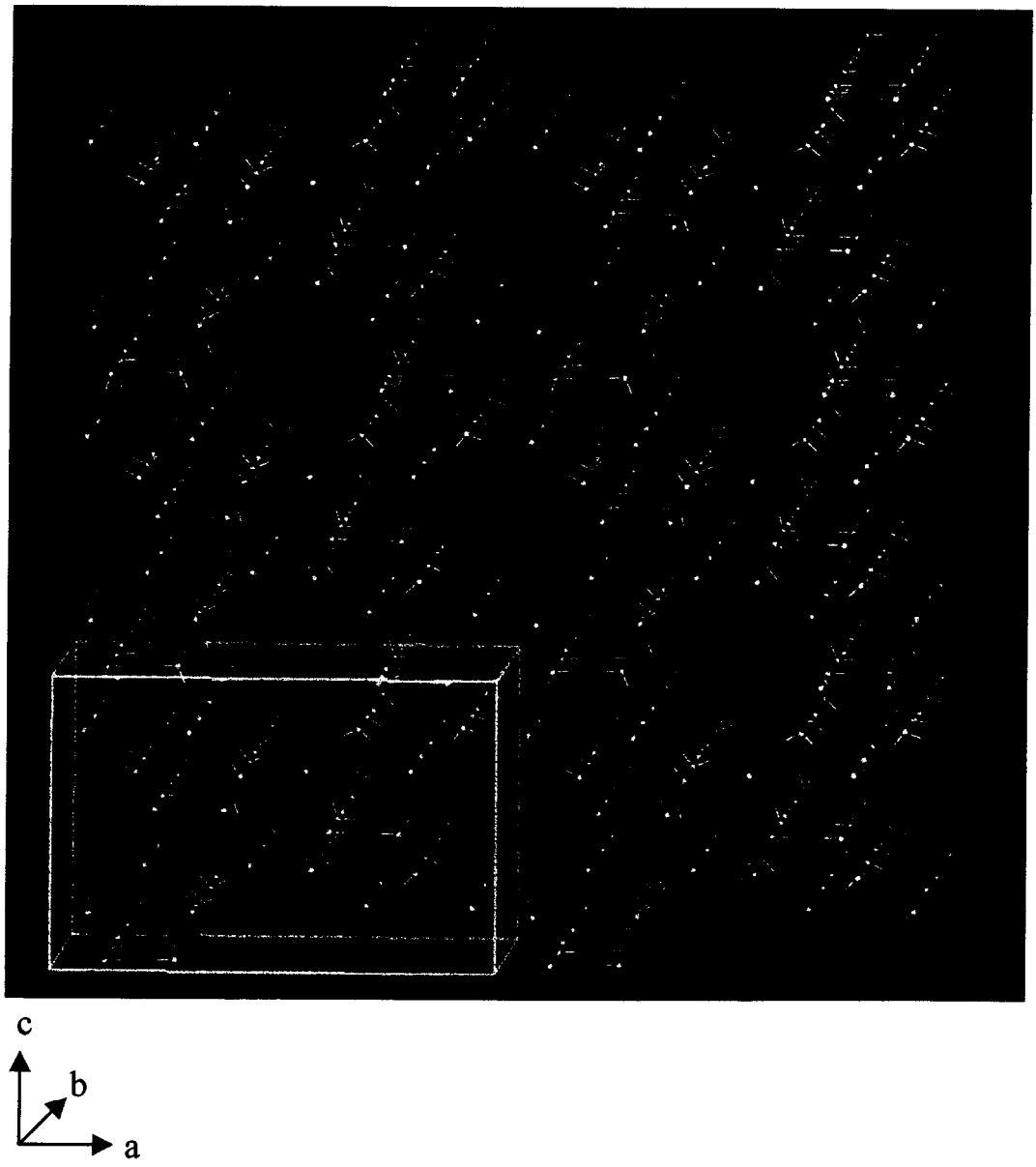

Fig. 1.6 A large MD simulation system for an MFI type zeolite. The system is composed of 2304 atoms (768 Si and 1536 O), corresponding to an array of $2 \times 2 \times 3$ crystal unit cells. Yellow and red spheres represent silicon and oxygen atoms, respectively. White lines indicate a crystal unit cell.

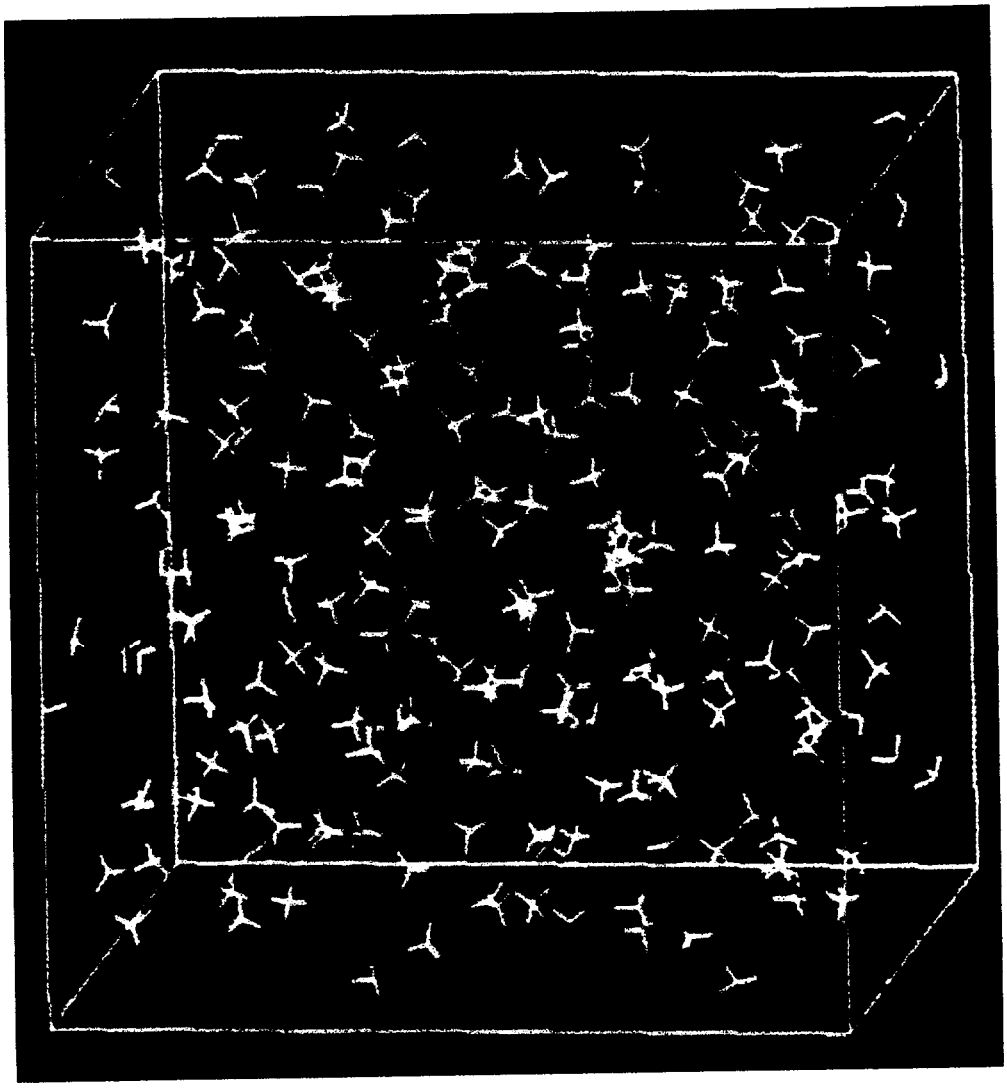

Fig. 1.7 An MD simulation cell of the initial structure for polymerization yielding gel. The system is composed of 1944 atoms (216 $Si(OH)_4$). Colored lines indicate bonds, where yellow and red represent silicon and oxygen atoms, respectively. Hydrogen atoms are omitted

Chapter 2

Thermal Behaviour of Silica Glass/Melt and Cristobalite

1. Introduction

Highly pure silica glass is used as crucibles and boats in the fabrication of semiconductor wafers. Its high viscosity prevents the distortion of such silicaware in high temperature use and its high purity avoids contamination to semiconductor wafers. Furthermore, it is used in industrial materials for optical fiber in long-distance telecommunication, because of its high transparency. The highly pure silica glass, thus, plays an important role in the present electronics and optoelectronics industries. The high temperature behaviour of thermal expansion, viscosity, and structural relaxation is important for the high temperature use and manufacture of various silica glass products. Their thermal history influences the ultimate properties such as mechanical strength and optical properties. Especially, the thermal behaviour around the glass transition temperature (T_g) and at higher temperatures is of practical importance.

It has been experimentally reported that the thermal expansion coefficient of the silica melt is negative in the temperature range from 1000 to 1550°C, and positive at higher temperatures [1]. The negative thermal expansion was connected to the negative thermal expansion of β-cristobalite, assuming the existence of the preordered regions that have properties very similar to cristobalite. Above 1550°C, "thermal decomposition" or "premelting" of the preordered regions takes place and the density-temperature curve behaves normally [1]. Recently, the existence of microcrystalline regions in the supercooled silica melt and glass has been suggested by the results of Rayleigh scattering [2]. The polarized scattering intensity drastically changes at the melting temperature of β-cristobalite, and the isothermal compressibility and the depolarization ratio are almost constant for the supercooled silica melt and glass. The relation between the assumed preordered regions and the microcrystalline regions has not been discussed yet.

Another possible explanation on the anomaly has been suggested by a molecular dynamics (MD) study about cooling-rate effects on the structure of amorphous silica [3]. It is based on the simulated results that densification and subsequent opening of the

tetrahedral network occurred with decreasing temperature. However, the relation between the anomaly and the negative thermal expansion of cristobalite has not been directly determined.

At temperatures below –80°C, silica glass also has a negative thermal expansion region. As with β-cristobalite, this anomaly has been attributed to the great freedom of transverse oxygen vibrations because of the openness of the structure [4]. In other words, if the structure has a vibrational mode whose frequency decreases as the structure shrinks, there will be a possibility of negative expansion. However, the negative thermal expansion of silica melt at higher temperatures has not been discussed. It should be considered that the transverse oxygen vibrations contribute to the thermal behaviour. In fact, the Si-O-Si bond angle was found to decrease by 1.3° when the fictive temperature increased from 950 to 1400°C, by examination of the shifts in bond stretching band [5]. X-ray diffraction has also demonstrated the decrease in the angle with increasing the fictive temperature from 1000 to 1500°C [6]. The variation in Si-O-Si angle is, thus, apparently consistent with the existence of the negative thermal expansion.

As described above, there are three structural problems to be considered for silica glass and melt, which are called amorphous silica hereafter: (1) Existence of the preordered regions having properties very similar to the corresponding crystal. (2) Changes in the tetrahedral network such as the ring size. (3) Effect of transverse oxygen vibrations as well as the variation in Si-O-Si angle. MD simulation is one of the most useful methods to understand the complicated thermal behaviour for amorphous and crystalline silica. Actually, MD simulations have been widely used in studies on the structures and dynamics of amorphous silica [7-9], cristobalite [10,11], and other forms of silica [12,13].

In the present study, we investigate some similarities of the thermal behaviour between amorphous silica and cristobalite using MD simulations, in order to understand the mechanism consistently from an atomistic point of view. The simulated thermal

behaviour of amorphous silica and cristobalite is also compared with experimental one to check the validity of the MD simulations.

2. Interatomic Potential Model

Interatomic potential functions used consist of Coulombic, short range repulsion, van der Waals attraction, and Morse potential terms. The Morse potential terms are applied only to the interactions between silicon and oxygen atoms,

$$U_{ij}(r_{ij}) = z_i z_j e^2/(4\pi\varepsilon_0 r_{ij}) + f_0(b_i+b_j)\exp[(a_i+a_j-r_{ij})/(b_i+b_j)] - c_i c_j / r_{ij}^6 + D_{ij}\{\exp[-2\beta_{ij}(r_{ij}-r^*_{ij})] - 2\exp[-\beta_{ij}(r_{ij}-r^*_{ij})]\} \quad (2,1)$$

where e is the elementary electric charge, ε_0 a dielectric constant of vacuum, r_{ij} an interatomic distance, and f_0 (=6.9511 $\times 10^{-11}$ N) a constant. Parameters, z, a, b, and c, are for atomic species, and D_{ij}, β_{ij}, r^*_{ij} are for Si-O pairs. These parameters were originally determined using MD simulations to reproduce the structures of various silica crystals such as quartz, cristobalite, and stishovite [11]. Furthermore, they have been adjusted to be consistently applicable to crystalline and amorphous silica, and mixtures of silica and water. The MD simulation of an MFI type zeolite gave a new insight into the structure and dynamics including the temperature-induced phase transition [12]. The parameters used in this study are listed in Table 2.1.

3. Molecular Dynamics Simulations

MD simulations were carried out using the MD program MXDORTO, developed by Kawamura [14]. The Ewald method was applied to the summation of Coulombic interactions. Newton's equations of motion were integrated with the velocity Verlet's algorithm using a time step of 2 fs. Temperature and pressure were controlled by scaling particle velocities and simulation cell constants, respectively. Temperature was varied over a range of 300-7000 K, and pressure was controlled at 1 atm. The system of 576 atoms (192 Si and 384 O), corresponding to an array of $4 \times 4 \times 3$ unit cells of α-cristobalite, was considered for cristobalite. Another system of 3000 atoms (1000 Si and 2000 O), corresponding to an array of $5 \times 5 \times 5$ unit cells of β-cristobalite, was used for amorphous silica. Periodic boundary conditions were adopted for both systems. The larger system was intended to reduce a finite size effect on structure and dynamics of amorphous silica. It has been reported that a simulation cell containing 3000 atoms are required to reproduce silica glass structures within 1% for different cooling cycles [15]. The simulation of cristobalite was started from an experimental structure of α-cristobalite [16], and then the system was heated up stepwise from 300 to 7000 K. At each temperature, time-averaged properties were evaluated for a run of 100 ps, following an equilibration run of 100 ps. The system for amorphous silica was equilibrated at 7000 K for 200 ps from the experimental structure of β-cristobalite [16], and then cooled to 300 K at a rate of 25 K/ps. At several temperatures on the cooling, the time-averaged properties were evaluated for a run of 100 ps, following an equilibration run of 100 ps.

4. Results

4.1. *Thermal Behaviour of Cristobalite*

The simulation system from the experimental structure of α-cristobalite shows a tetragonal lattice below 450 K, and the lattice changes into a cubic one at 500 K as shown in Fig. 2.1. This change in lattice shape is corresponding to the experimental α-β phase transition [16, 17]. The phase transition has been experimentally observed with different specimens in the temperature range from 393 to 545 K [18]. The other characteristics of thermal behaviour are also reproduced; α-cristobalite has positive thermal expansion with the largest elongation along c axis, whereas β-cristobalite has negative thermal expansion. The quantitative difference in lattice constants and thermal expansion coefficients will be discussed in Section 5.3.

As shown in Fig. 2.2, the average Si-O-Si angle drastically increases during the α-β transition. The angle increases with temperature for α-cristobalite, but decreases for β-cristobalite before melting at 5000 K. The average O-Si-O angle changes only a little. Fig. 2.3 shows temperature dependence of the average distances between the nearest neighbor atoms, defined by the first peak positions of pair correlation functions $g_{ij}(r)$. The distances for Si-O and O-O increase with temperature and the variations are smaller than that for Si-Si. Therefore, the lattice constants for cristobalite shows the same temperature dependence as the nearest Si-Si distances and the Si-O-Si angle; the former is governed by the latter because the variation in the Si-O distance is very small.

Fig. 2.4 shows temperature dependence of the components of potential energy. The total potential energy (U_{total}) is divided into the Coulombic energy (U_{Coulomb}) and short range energy (U_{short})

$$U_{\mathrm{total}} = U_{\mathrm{Coulomb}} + U_{\mathrm{short}} = U_{\mathrm{Coulomb}} + [U_{\mathrm{vdW}} + U_{\mathrm{srr}} + U_{\mathrm{Morse}}] \qquad (2.2)$$

where U_{vdW}, U_{srr} and U_{Morse} indicate van der Waals attraction, short range repulsion, and Morse potential energies, respectively. The Coulombic energy decreases by 9.9 kJ/mol

during the α-β transition. Considering the variations in the distances for the nearest atom pairs in Fig. 2.3, the decrease in the Coulombic energy is due to the expansion of the Si-Si distance. The energy increases monotonically with temperature below and above the transition temperature, owing to the expansion of Si-O and the contraction of Si-Si, respectively. The short range energy increases by 10.9 kJ/mol during the α-β transition because of the reduction in the van der Waals attraction energy between oxygen atoms. The second peak of $g_{OO}(r)$ shifts from 3.83 to 4.55 Å as shown in Fig. 2.5. The energy slightly increases with temperature before and after the α-β transition owing to the expansion of the O-O distance. The enthalpy of the α-β transition is estimated to be 0.9 kJ/mol at 450 K, which is in reasonable agreement with the experimental value of 1.3 kJ/mol at 523 K [19].

The mean square displacements (MSDs) of atoms are shown in Fig. 2.6. The MSDs sharply increase during the α-β transition and after that the slopes become steeper, especially for oxygen atoms.

4.2. Thermal Behaviour of Amorphous Silica

Fig. 2.7 shows variation in density for cristobalite on heating and for amorphous silica on cooling. Variation in enthalpy is also shown in Fig. 2.8 for both forms of silica. β-cristobalite melts at 5000 K with a drastic increase in density and enthalpy. The density curve of silica melt exhibits a maximum at 5200 K and a minimum at 3800 K. The enthalpy curve is almost linear in the high temperature range including the temperature of the density maximum, and shows an inflection at 3800 K indicating the glass transition. The density maximum of silica melt has been experimentally observed at 1550°C, which is higher than the glass transition temperature of about 1200 K and lower than the melting point of cristobalite [1]. The present simulation overestimates both the melting point and the glass transition temperature, unlike the α-β transition of cristobalite. The overestimation will be discussed in Section 5.3.

The temperature dependence of bond angles for amorphous silica is shown in Fig.

2.2 with that for cristobalite. The drastic decrease in the average Si-O-Si angle is found at the temperature corresponding to the melting of cristobalite, which is correlated with the drastic increase in density as shown in Fig. 2.7. Too large variation in the average Si-O-Si angle will be discussed in Section 5.3. The average O-Si-O angle for amorphous silica varies a little and shows a minimum around the temperature of the density maximum, while the average Si-O-Si angle increases monotonously with decreasing temperature. The temperature dependence of the average Si-O-Si angle is consistent with the experimental result [5]. In the temperature range from 500 to 4800 K, both the curves of bond angles have negative slopes like those of β-cristobalite. The variation in the average Si-O-Si angle does not correspond to the variation in density, in contrast to that found for cristobalite. Fig. 2.9 shows $g_{SiSi}(r)$ and the integrated coordination numbers $n_{SiSi}(r)$ for amorphous silica at several temperatures. Fig. 2.10 shows the temperature dependence of $n_{ij}(r)$ at the following characteristic distances r: 2.14 Å for Si-O, 2.96 Å for O-O, and 3.39, 6.09 and 8.49 Å for Si-Si. The distances for Si-O and O-O are the positions of the first minimum in $g_{ij}(r)$ at 300 K. The distances for Si-Si are indicated in Fig. 2.9, which are the first, second, and third minima in the $g_{SiSi}(r)$ at 300 K, excluding the minimum at 4.8 Å that disappears at higher temperatures. The average number of oxygen atoms around a silicon atom, $n_{SiO}(2.14)$, increases up to 4.0 when silica melt is cooled to 4000 K, followed by leveling off. The quantities $n_{OO}(2.96)$ and $n_{SiSi}(3.39)$ increase monotonically with decreasing temperature. The value of $n_{OO}(2.96)$ above 6.0 suggests the contribution of the second or third nearest neighbor oxygen atoms by deformation of ring structure. The quantities $n_{SiSi}(6.09)$ and $n_{SiSi}(8.49)$ exhibit a maximum at 5000 K and a positive slope in the temperature range from 3000 to 5000 K like the density curve for amorphous silica shown in Fig. 2.7.

In order to clarify the temperature dependence of the intermediate range structure in the scale larger than 3.39 Å, the size distribution curves of network-forming rings at several temperatures are shown in Fig. 2.11. The ring size stands for the number of

silicon atoms constituting a ring. At 7000 K, the total number of rings is the smallest and 3- to 5-membered rings are predominant. With decreasing temperature, the total number of rings increases and 5- to 7-membered rings become dominant.

Finally, the mole fractions of three major species in different coordination states are shown in Fig. 2.12 as a function of temperature. The other species are omitted because of the mole fractions less than 0.02. The threshold distance of 2.2 Å, where the integrated coordination number $n_{SiO}(r)$ is four below the glass transition temperature, is used to determine a coordination number for each atom. The fixed threshold distance is adopted to relate the coordination number to density. The silicon atoms coordinated with five oxygen atoms and the oxygen atoms coordinated with three silicon atoms are called overcoordinated species. The silicon atoms coordinated with three oxygen atoms and the oxygen atoms coordinated with a silicon atom are called undercoordinated species. Each defect decreases with decreasing temperature and disappears around 3000 K.

5. Discussion

5.1. Thermal Behaviour and Atomistic Structure for Cristobalite and Glass

The thermal expansion coefficient of α-cristobalite, a high density phase, is positive, while that of β-cristobalite, a low density phase, is negative in Fig. 2.7. The thermal expansion coefficient of silica glass having density close to α-cristobalite is positive. The difference in density expresses the extent of openness or compactness, which affects the mobility of atoms, as shown in Fig. 2.6. Two kinds of atoms in α-cristobalite and silica glass are prevented from moving about by the surrounding atoms, as compared with those in β-cristobalite. In this section, the relation between thermal expansion and atomistic structure is first discussed for cristobalite, and then for silica glass.

For cristobalite, the thermal expansion is correlated to both the average Si-O-Si angle and the related first peak position of $g_{SiSi}(r)$, as shown in Figs. 2.2 and 2.3. These variations with increasing temperature are positive for α-cristobalite and negative for β-cristobalite. For α-cristobalite having the compact structure, increasing the repulsion between atoms with thermal motion brings about the normal thermal expansion. For β-cristobalite having the bulky structure, the MSD for oxygen atoms is much larger than that for α-cristobalite. Therefore, the anomaly, negative thermal expansion, would be attributed to the great freedom of transverse oxygen vibrations. This is consistent with the previous conclusion from the calculation using a simple model [4].

For silica glass, the density increases with temperature in despite of decreasing the average Si-O-Si angle in Fig. 2.7. This situation is different from that of cristobalite. The broad distribution of the ring size leads silica glass to less compact structure than α-cristobalite. The integrated coordination numbers except $n_{SiO}(r)$ for silica glass decrease with temperature in Fig. 2.10. It should be noted that the value of $n_{OO}(2.96)$ more than 6.0 in the low temperature range arises from the deformation of the rings followed by the approach of the second or third nearest oxygen atoms. Silica

glass eventually has positive thermal expansion, because the effect of ring deformation surpasses that of the Si-O-Si angle contributing to negative thermal expansion.

5.2. Thermal Behaviour and Atomistic Structure for Silica Melt

The temperature dependence of density for silica melt exhibits a maximum at 5000 K and a positive slope, i.e. negative thermal expansion, in the temperature range from 3800 (T_g) to 5000 K, as shown in Fig. 2.7. The characteristic behaviour is explained by the change in the network structure (densification and opening).

In Fig. 2.12, there are a large number of the undercoordinated species. These species are consumed to form the regular ones with decreasing temperature. The increase in the average coordination number, namely, the progress in the bond formation contributes to the densification (normal thermal expansion).

In Fig. 2.10, only the integrated coordination numbers, $n_{SiSi}(6.09)$ and $n_{SiSi}(8.49)$, have the same temperature dependence as density. Furthermore, the number of 5- to 7-membered rings increases, whereas the number of the smaller 2- and 3-membered rings decreases with decreasing temperature, as shown in Fig. 2.11. Therefore, the negative thermal expansion is related to the intermediate range structure in the scale larger than 3.39 Å, indicating network opening. The structural rearrangement suggests that the network structure of silica melt approaches that of cristobalite built by only 6-membered rings.

These results lead to the conclusion that two opposite factors cause the maximum in the temperature dependence of density for silica melt: with decreasing temperature, densification due to the increase in the number of bridging bonds, and opening of the tetrahedral network due to the rearrangement of network-forming rings.

5.3. Quantitative Differences in Results between Simulations and Experiments

Some quantitative deviations from the experimental results were found in the lattice constants, the density, and the temperatures of the thermal events (melting, glass transition, and the density maximum) for cristobalite and amorphous silica, as described in Section 4. In this section, the causes of the differences are discussed.

Table 2.2 shows the simulated and experimental results of the local structures and the density. These values for α-cristobalite fairly agree with each other. On the other hand, the density is lower for β-cristobalite and higher for silica glass than the experimental one. In addition, the larger temperature dependence of lattice constants is simulated for cristobalite in Fig. 2.1.

For β-cristobalite, the bond distance of Si-O, the interatomic distance of O-O, and hence the average O-Si-O angle are consistent with observations, whereas the average Si-O-Si angle and hence the interatomic distance of Si-Si are larger than the experimental ones. This is attributed to the problem in the interatomic potential model concerning the Si-O-Si angle, which is too much flexible. Similar situation, however, is not seen for α-cristobalite. For a bulky phase, β-cristobalite, the density is underestimated by the overflexibility of the Si-O-Si angle. The temperature dependence of density is also correlated with that of the average Si-O-Si angle in Figs. 2.2 and 2.7. As a result of this, the thermal expansion is overestimated.

For silica glass, the average Si-O-Si angle deviates from the experimental one, whereas the bond distance of Si-O and the average O-Si-O angle are reproduced well. These results are apparently contradictory to those of the interatomic distances of O-O and Si-Si. This can be understood from the ring structure as follows. For the melt, the number of small rings increases with temperature in Fig. 2.11. The change is consistent with the decrease in the Si-O-Si angle. Because of the overflexibility of the Si-O-Si angle, the number of small rings would be overestimated than that of a real system. From such melt, the simulated glass was made by extremely rapid cooling

process. The structure seen in the melt would be frozen without enough restructuring the rings to 6-membered rings [3]. This is the reason why the deviations from observations occur in local structure. Furthermore, the different situation between the O-O distance and the Si-Si distance is due to the following; oxygen atoms can approach with each other closer than silicon atoms, because the interatomic interaction of O-O is more attractive than that of Si-Si in the Coulombic repulsion and the van der Waals attraction. The larger cause of overestimation of density for silica glass is ultimately the overflexibility of the Si-O-Si angle. In the same way of this, the density for silica melt would be overestimated with the drastic decrease in the average Si-O-Si angle during melting of cristobalite in Fig. 2.2. The interatomic potential model concerning Si-O-Si angle can be improved by the addition of a three-body potential term for the bond angle constraint, if necessary.

The simulated melting temperature of cristobaite, 4900 K, is much higher than the measured temperature of 1996 K [19]. The discrepancy could result from the very high heating rate, the absence of defects and surfaces, and the overestimation of bond energy. The glass transition temperature of 3800 K and the density maximum temperature of 5200 K from this simulation are also much higher than the experimental ones of about 1470 and 1820 K, respectively [1]. So far MD simulations have predicted too high glass transition temperatures: 2200 K [9], 3000 K [7], 2900-3250 K depending on the cooling rate [3], and others. The reasons could be the very high cooling rate, the finite size of simulation cell with periodic boundary conditions, and the overestimation of bond energy.

6. Conclusion

The MD simulations reproduce the α-β phase transition of cristobalite, the negative thermal expansion of β-cristobalite, and the density anomaly of the silica melt. The thermal expansion of cristobalite is closely related to the distances between the nearest neighbor silicon atoms originating from the Si-O-Si angle. On the other hand, the thermal expansion of amorphous silica is governed by the longer-range structure, the network-forming rings. Therefore, the density of silica glass increases with temperature because of the ring deformation in despite of a decreasing average Si-O-Si angle. Furthermore, the density anomaly of the silica melt is caused by two opposite factors in the density variation with decreasing temperature: densification due to the increase in number of bridging bonds, and opening of the tetrahedral network due to the rearrangement of network-forming rings. Finally, the main structural changes governing the thermal expansion are summarized for both cristobalite and amorphous silica in Fig. 2.13.

References

[1] R. Brückner, J.Non-Cryst.Solids, 5 (1970) 123.

[2] K. Saito, H. Kakiuchida, A. J. Ikushima, J. Non. Cryst. Solids, 222 (1997) 329.

[3] K. Vollmayr, W. Kob, and K. Binder, Phys. Rev. B, 54(22) (1996) 15808.

[4] H.T. Smyth, J. Am. Ceram. Soc., 38 (1955) 140.

[5] A. Agarwal, K. M. Davis, and M. Tomozawa, J. Non-Cryst. Solids, 185 (1995) 191.

[6] V.E. SokoI'ski, V.A. Shovskii, V.P. Kazimirov, and G.I. Batalin, Soc. J. Glass Phys. Chem. (Transl.) 6 (1980) 338.

[7] Y. Benino, K. Hirao, N. Soga, J. Non-Cryst. Solids, 183 (1995) 22.

[8] L.V. Woodcock, C.A. Angell and P. Cheeseman, J. Chem. Phys., 65 (1976) 1565; T.F. Soules, J. Non-Cryst. Solids, 73 (1985) 315; J. Horbach, W. Kob, and K. Binder, Philosophical Magazine B, 77, 2 (1998) 297; P.H. Poole, M. Hemmati, and C. A. Angell, Phys. Rev. Lett., 79 (1997) 2281; P. Vashishta, R.K. Kalia, and J.P. Rino, Phys. Rev. B, 41, 17(1990) 12197.

[9] R.G.D. Valle and H.C. Andersen, J. Chem. Phys., 97 (4) (1992) 15

[10] L. Duffrène and J. Kieffer, J. Phys. Chem. Solids, 59, 6-7 (1998) 1025; J.S. Tse and D.S. Klug, J. Chem. Phys., 95 (1991), 9176.

[11] K. Kawamura, in: Molecular Dynamics Simulations, ed. F. Yonezawa (Springer-Verlag, Berlin, 1990) p. 88.

[12] K. Yamahara, K. Okazaki, K. Kawamura, Catalysis Today, 23 (1995) 397.

[13] S. Tsuneyuki, M. Tsukada, H. Aoki, and Y. Matsui, Phys. Rev. lett., 7 (1988) 869; S. Tsuneyuki, Y Matsui, H. Aoki, M. Tsukada, Nature, 339 (1989) 209; A.B. Belonoshoko and L.S. Dubrovinsky, Geochimica et Cosmochimica Acta, 59, No. 9 (1995) 1883; V.V. Murashov and I.M. Svishchev, Phys. Rev. B, 57, 10 (1998) 5639.

[14] K. Kawamura, MXDORTO, Japan Chemistry Program Exchange, #029; K. Kawamura, JCPE Newslett., 5 (2) (1993) 30.

[15] N.T. Huff, E. Demiralp, T. Çagin, and W.A. Goddard III, J. Non-Cryst. Solids, 253 (1999) 133.

[16] D.R. Peacor, Z.Kristallogr., 138 (1973) 274.

[17] K. Ohsumi, T. Sawada, Y. Takeuchi, and R. Sadanaga, in: Materials Science of the Earth's Interior, ed. I. Sunagawa (Terra Scientific Publishing Company, Tokyo, 1984) p. 633.

[18] R.B. Sosman, The Phases of Silica (Rutgers University Press, New Brunswick, 1965).

[19] R.A. Robie, B.S. Hemingway, and J.R.Fisher, Thermodynamic Properties of Minerals and Related Substances at 298.15 K and 1 Bar Pressure and at Higher Temperatures (United States Government Printing Office, Washington, 1978) p. 217.

[20] R.L. Mozzi, B.E. Warren, J. Appl. Cryst., 2 (1969) 164.

Table 2.1 Parameters for the interatomic potential model.

Atom	z	a (Å)	b (Å)	c ($kJ^{1/2}$ Å $^3mol^{-1/2}$)
O	-1.2	1.926	0.160	40.9
Si	2.4	0.945	0.090	0.0

Atom pair	D (10^{-19}J)	β ($Å^{-1}$)	r^* (Å)
Si-O	5.14	2.0	1.51

Table 2.2 Simulated and experimental interatomic distances* (Å), bond angles (°), and density (g/cm^3).

	Interatomic distance				Bond angle		
	T (K)	Si-O	O-O	Si-Si	O-Si-O	Si-O-Si	Density
Glass							
MD	300	1.60	2.60	3.13	109.36	146.51	2.44
X-ray [20]	300	1.62	2.65	3.12	109.8	144	2.20
α-Cristobalite							
MD	300	1.60	2.61	3.07	109.42	146.99	2.38
X-ray [16]	301	1.61	2.63	3.08	109.7	146.4	2.33
β-Cristobalite							
MD	500	1.60	2.62	3.18	109.43	165.37	2.02
X-ray [16]	494	1.615		3.10		147.7	2.18

*Simulated bond distances are defined as the first peak positions in pair correlation functions.

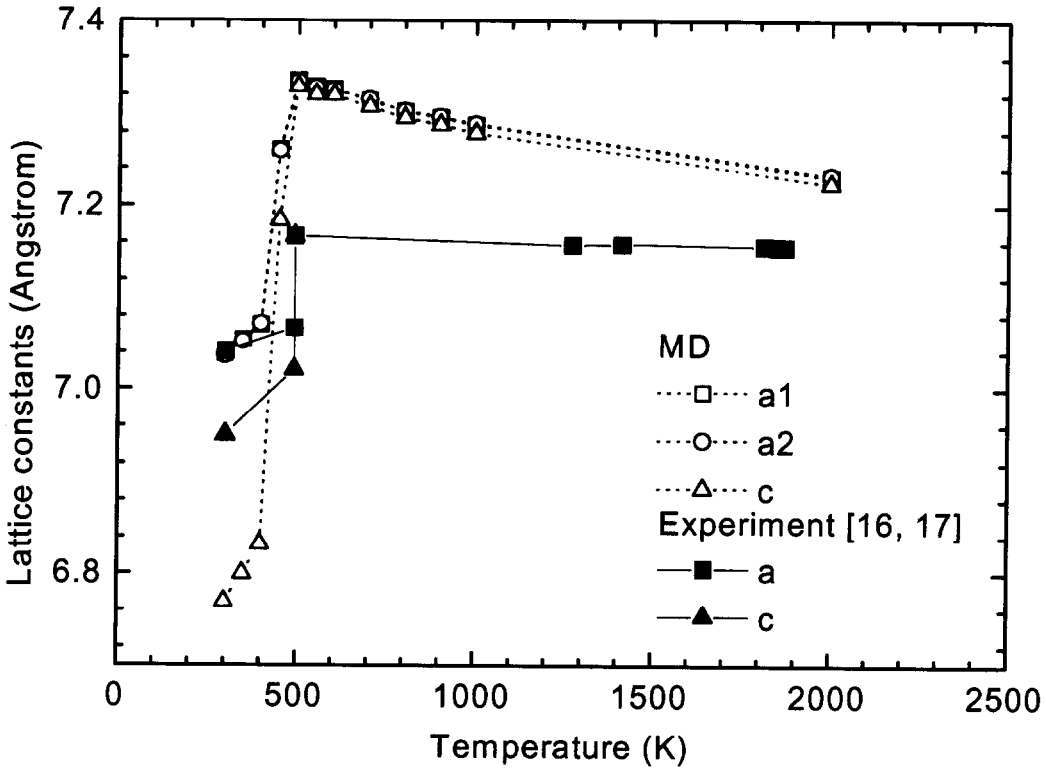

Fig. 2.1 Simulated and experimental lattice constants of cristobalite. The MD simulation distinguishes between the two equivalent lattice constants, a1 and a2, of tetragonal systems.

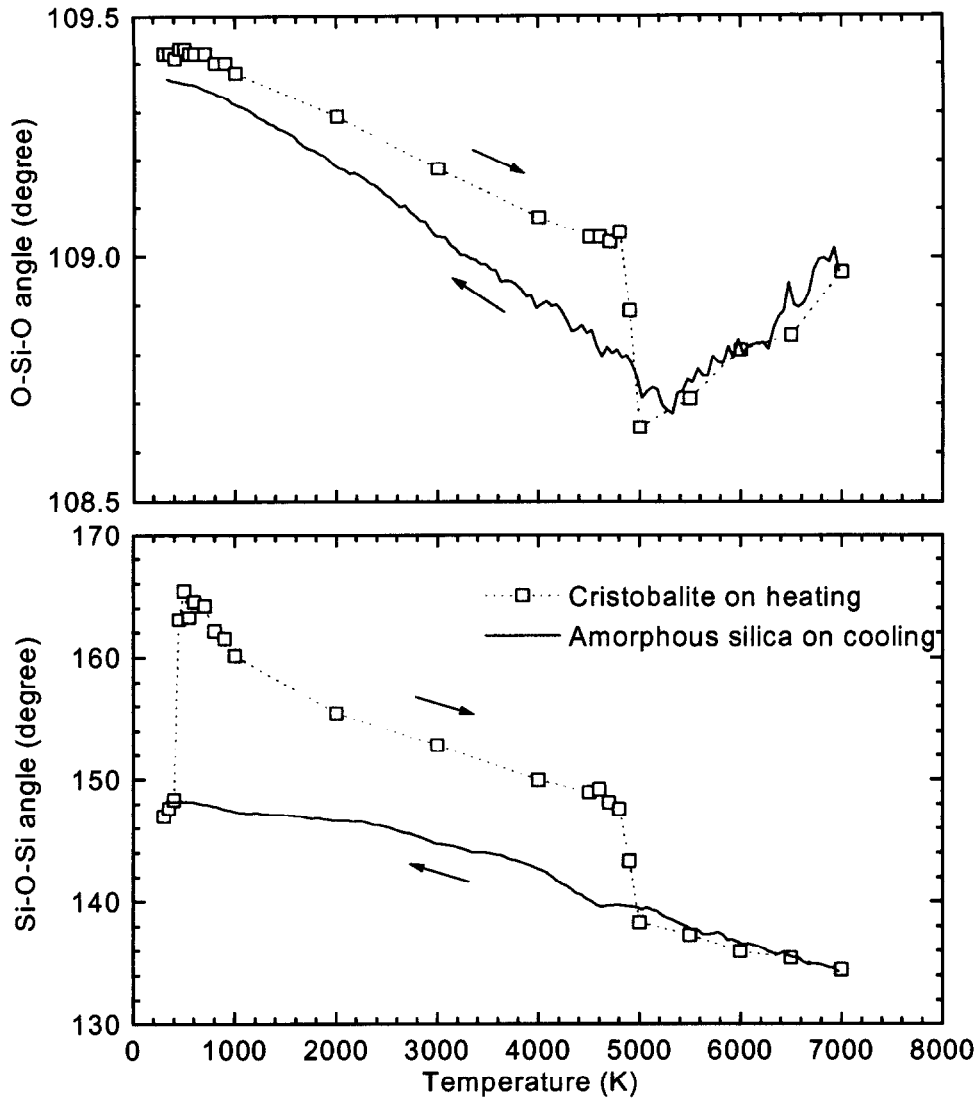

Fig. 2.2 Bond angles of cristobalite and amorphous silica as a function of temperature. Cristobalite is on heating, whereas amorphous silica is on cooling. Note that the scale on the ordinate for each graph is different.

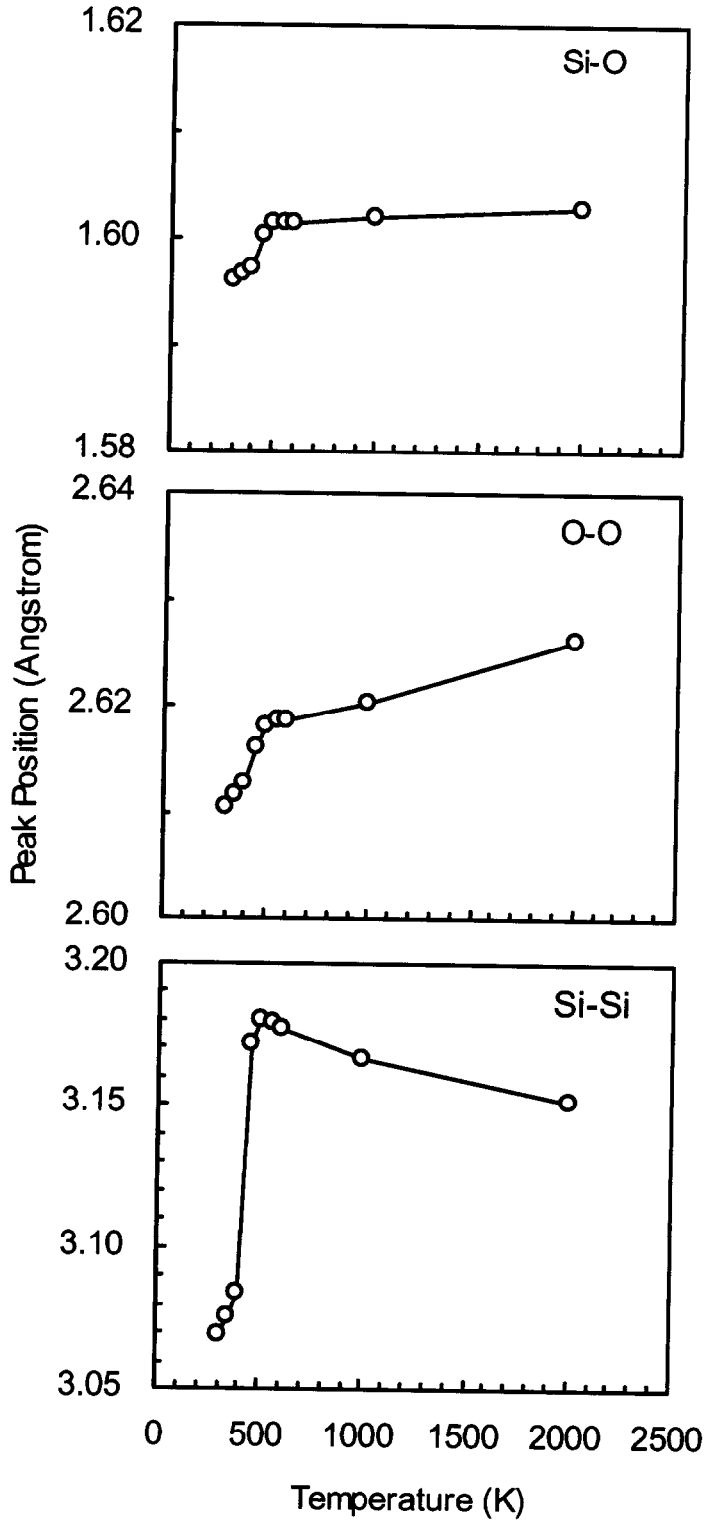

Fig. 2.3 The first peak positions of pair correlation functions, $g_{SiO}(r)$, $g_{OO}(r)$, and $g_{SiSi}(r)$, for cristobalite as a function of temperature. Note that the scale on the ordinate for each graph is different.

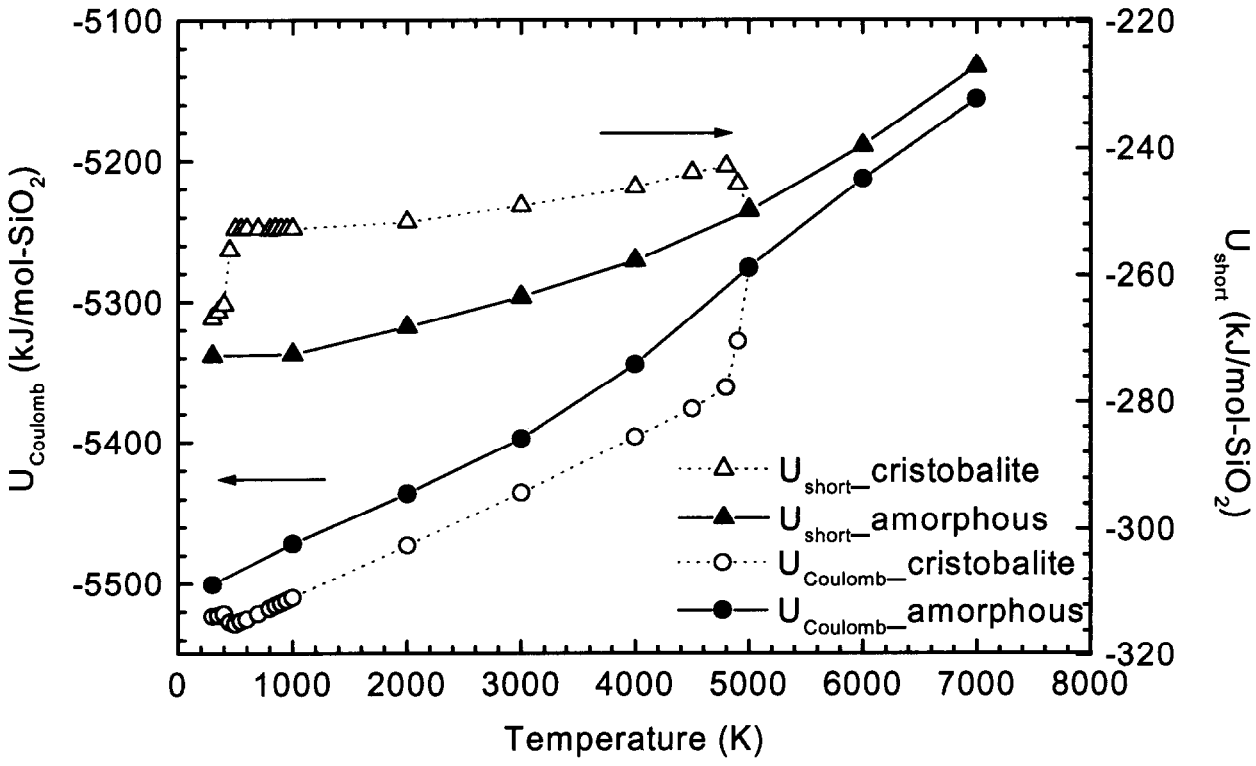

Fig. 2.4 Coulombic (U_{Coulomb}) and short range (U_{short}) energies for cristobalite and amorphous silica as a function of temperature.

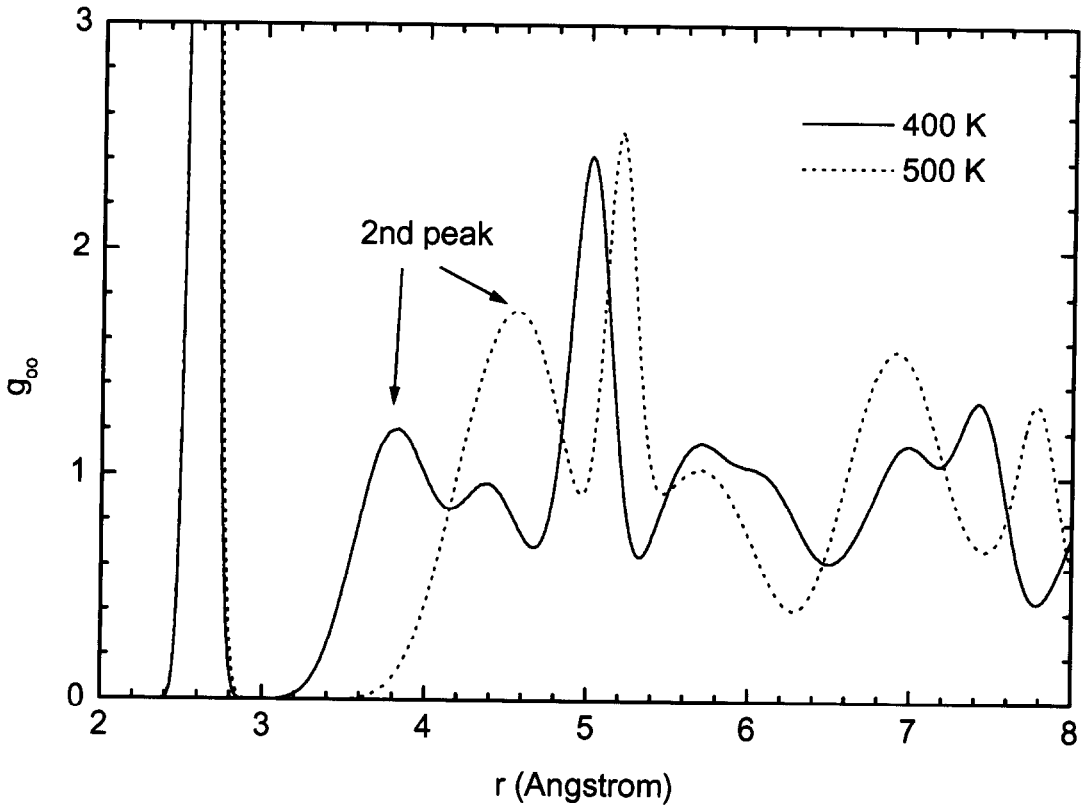

Fig. 2.5 Pair correlation function $g_{OO}(r)$ for cristobalite at the temperatures below and above the α-β transition.

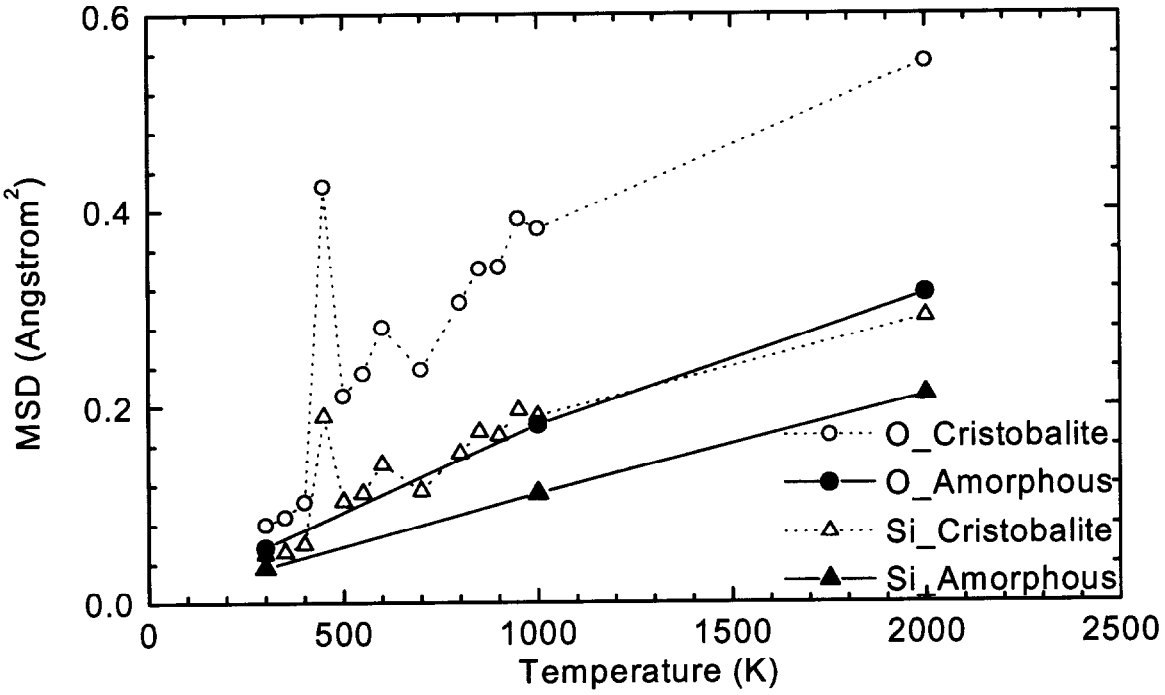

Fig. 2.6 Mean square displacements from the initial positions of atoms in cristobalite and amorphous silica as a function of temperature.

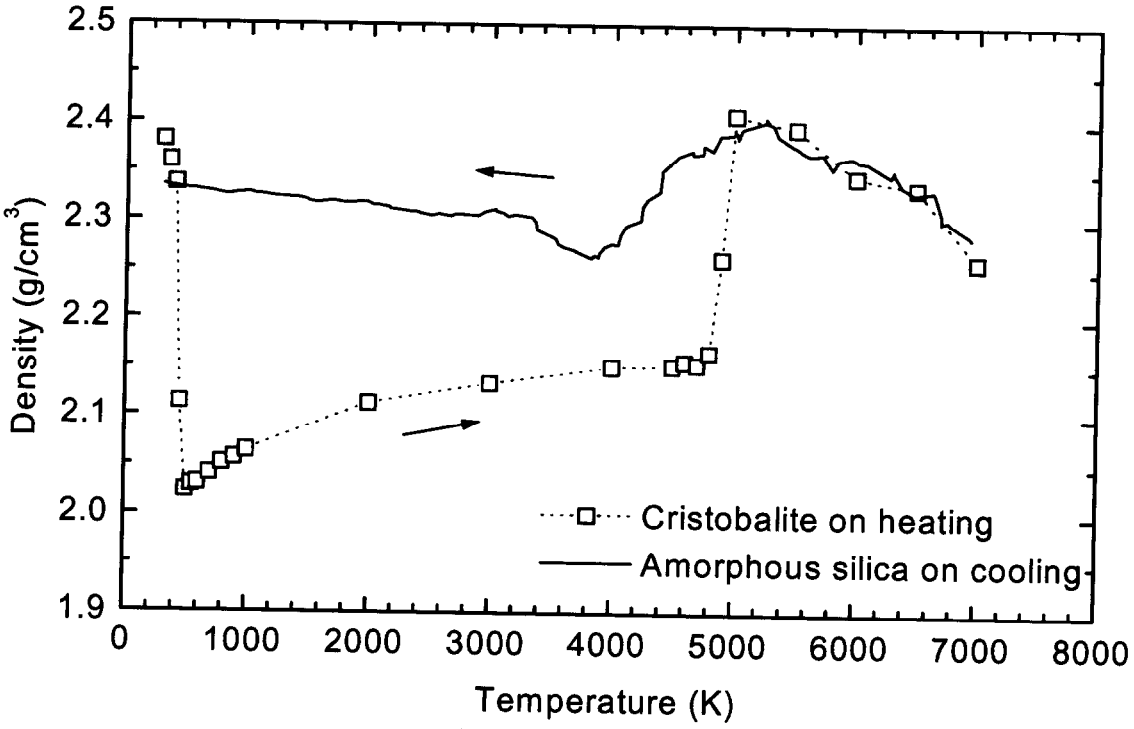

Fig. 2.7 Temperature dependence of density for cristobalite and amorphous silica. Cristobalite is on heating, whereas amorphous silica is on cooling.

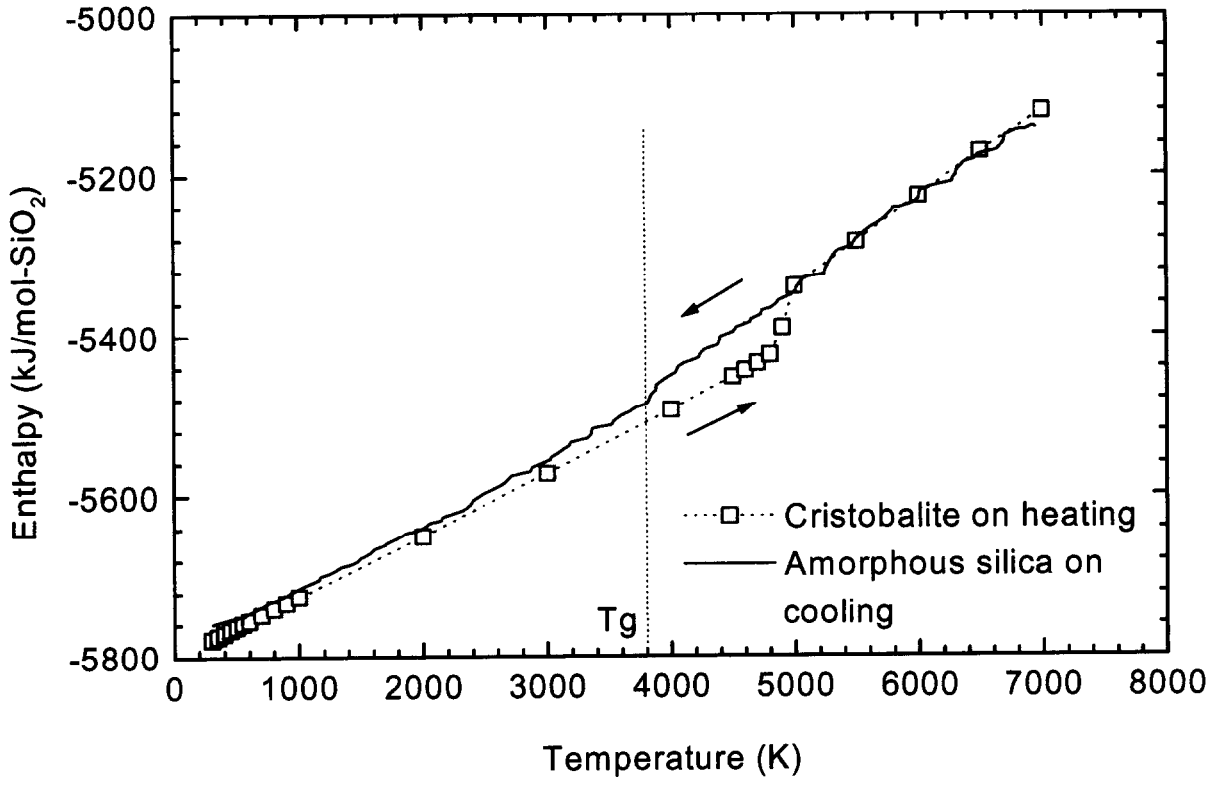

Fig. 2.8 Temperature dependence of enthalpy for cristobalite and amorphous silica. Cristobalite is on heating, whereas amorphous silica is on cooling.

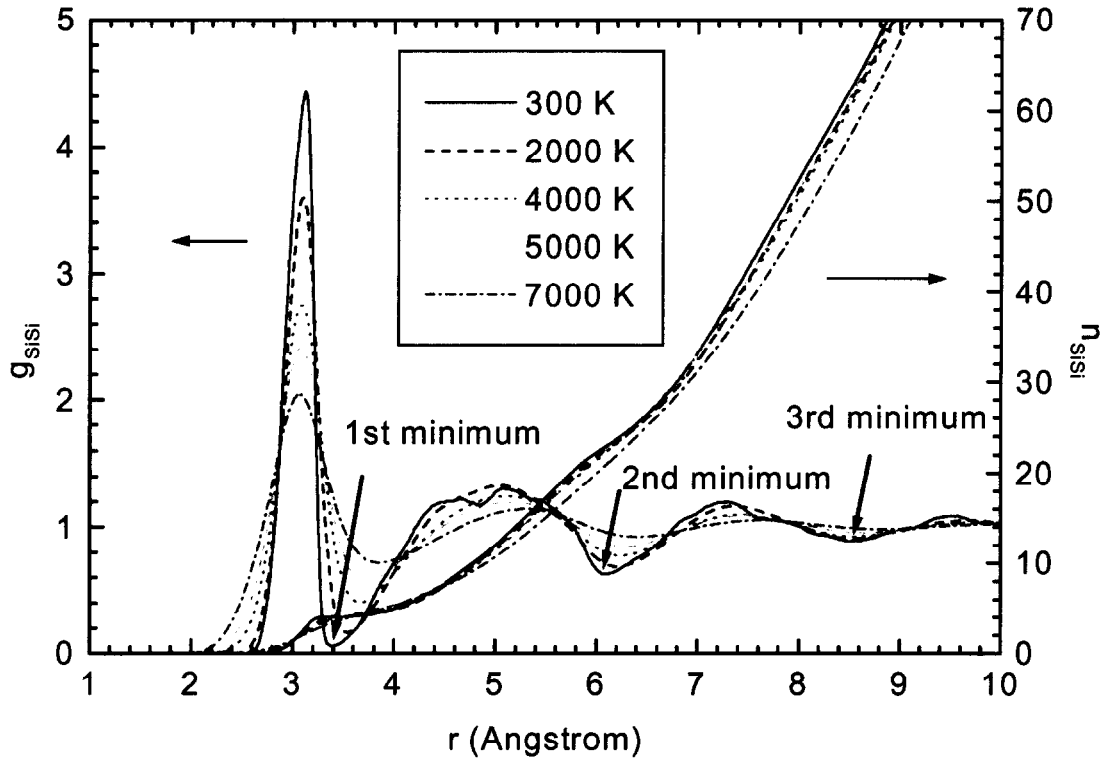

Fig. 2.9 Pair correlation functions $g_{SiSi}(r)$ and integrated coordination numbers $n_{SiSi}(r)$ for amorphous silica at several temperatures.

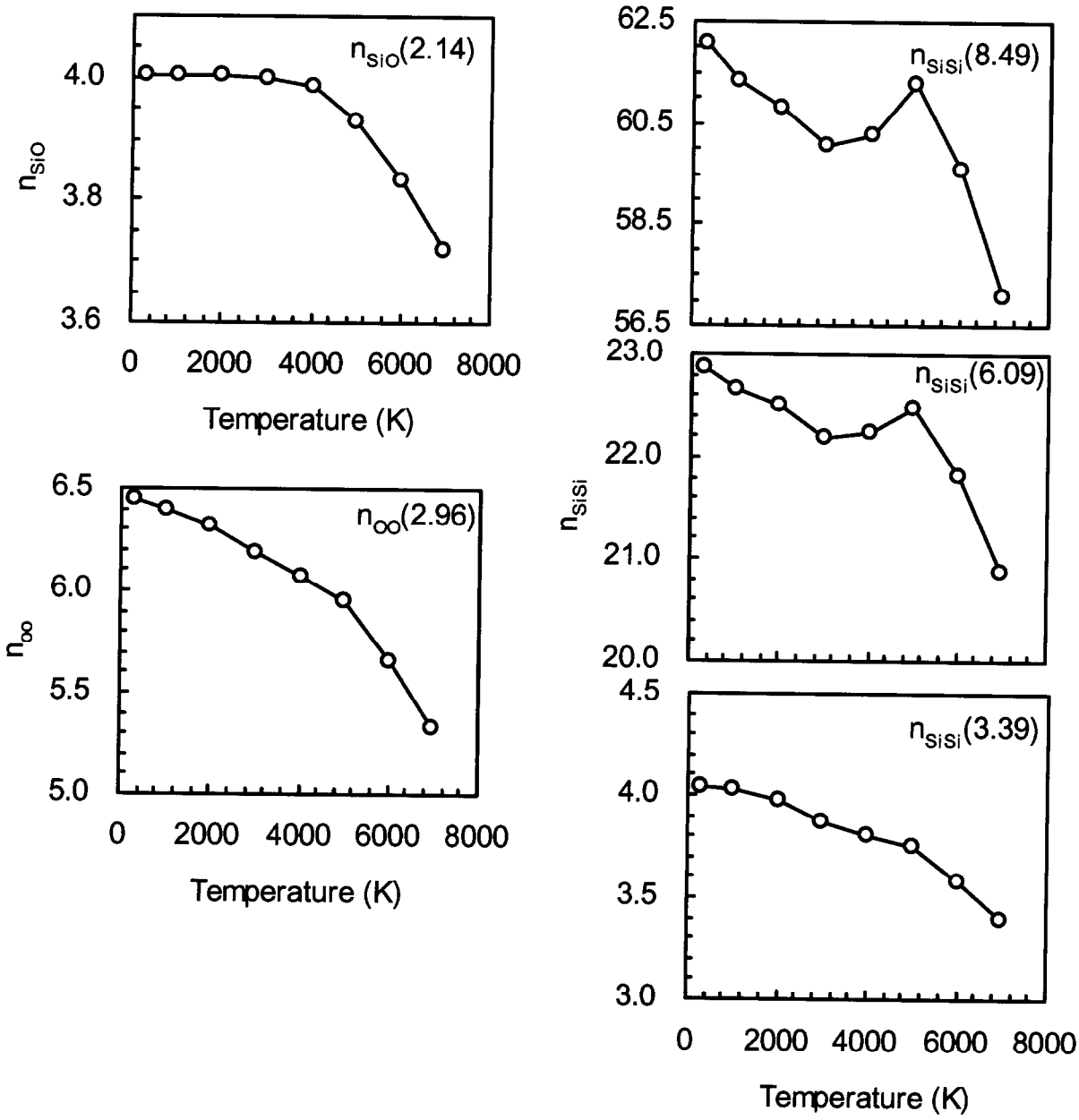

Fig. 2.10 Integrated coordination numbers $n_{ij}(r)$ for amorphous silica as a function of temperature.

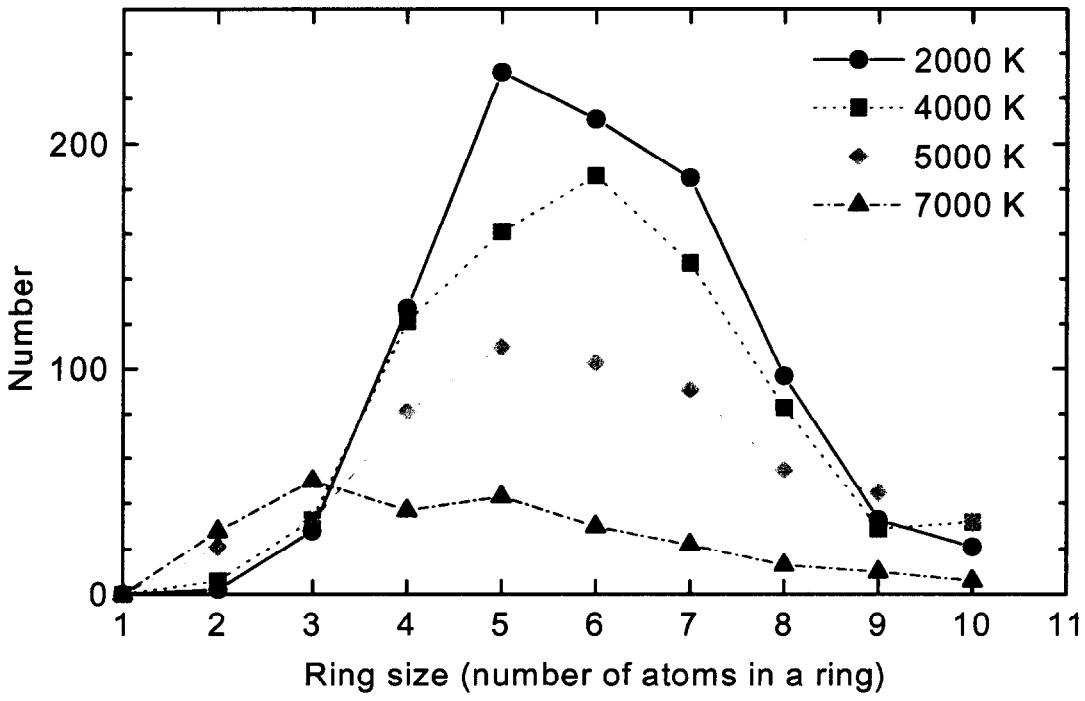

Fig. 2.11 Ring size distribution for amorphous silica at several temperatures.

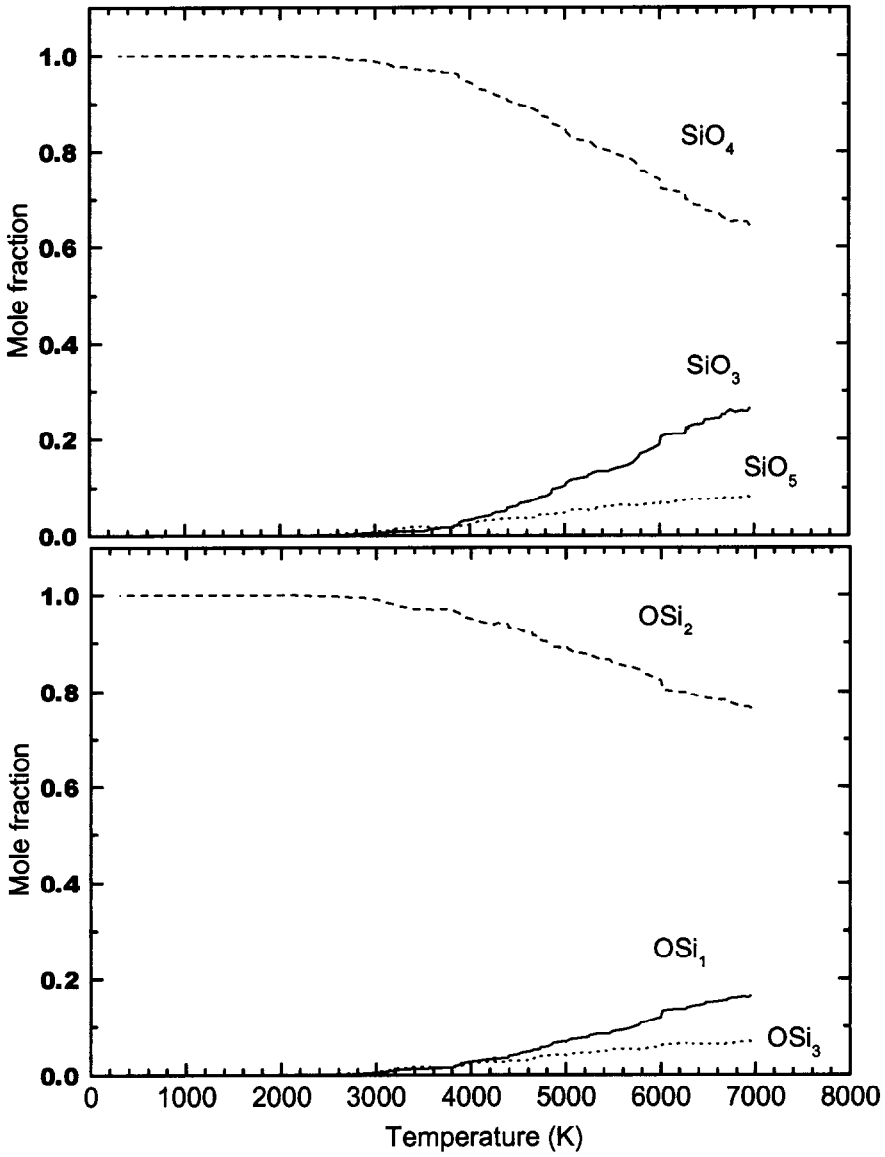

Fig. 2.12 Mole fractions of silicon (upper) and oxygen (lower) atoms with different coordination states for amorphous silica as a function of temperature.

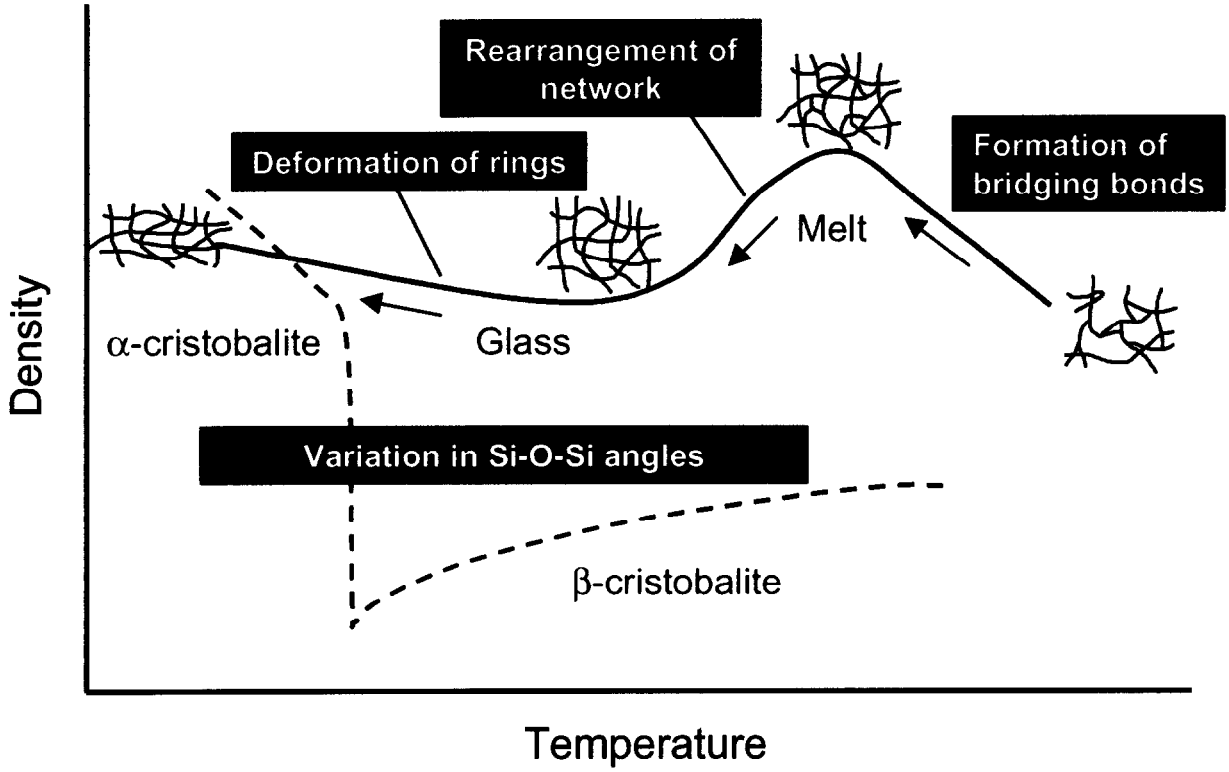

Fig. 2.13 Dominant factors of the density behaviour for cristobalite and amorphous silica. The network structure for amorphous silica is schematically illustrated, where lines and intersections indicate bridging bonds and silicon atoms, respectively.

Chapter 3

Thermal Behavior of an MFI-type Zeolite

1. Introduction

Zeolites are generally crystalline aluminosilicates. Their frameworks, composed of interconnected TO_4 (T=Si, Al) tetrahedral networks, have numerous molecular dimensional micropores. These channels give rise to characteristic properties of zeolites such as the molecular sieve effect and the shape selective catalysis. It is known that zeolite frameworks should not only vibrate thermally, are also often distorted by phase transitions induced by the presence of sorbed molecules or temperature. It is thus meaningful to model the flexible frameworks in a simulation in order to understand the properties of the zeolites.

MFI-type zeolites have a high Si/Al ratio. A siliceous MFI compound called silicalite is used as a molecular sieve. Other MFI materials called ZSM-5 have been of great interest in recent years because of their high catalytic activity and excellent shape selectivity. They are widely used as industrial catalysts. Several investigations by X-ray diffraction [1-6], as well as NMR [7,8], indicate that MFI-type zeolites show a reversible phase transition. The phase transition temperature depends on the content of aluminum or other substituted elements [3,4]; The temperature is reported as being about 340 K for H-ZSM-5 [2], while it increases up to 511 K for (Ge)-ZSM-5 [3]. X-ray diffraction showed that the space group symmetries are orthorhombic *Pnma* [2-6, 9, 10] and monoclinic $P2_1/n$ [1], above and below the phase transition temperature, respectively.

There are a few simulation studies with respect to this phase transition. Bell et al. [11] reported that lattice energy minimization calculations, performed with the orthorhombic structure of silicalite as an initial structure, result in the simulation of the low-temperature monoclinic phase. Burchart et al. [12] also examined this phase transition by lattice energy minimization calculations using their original all-silica force fields. Their results slightly differ from those of Bell et al. in that they obtained both phases as energy minimum. Although MD simulations were applied by Demontis et al.

[13], the phase transition could not be reproduced. They attributed this to the quality of the potential model.

In the present work, we have carried out MD simulations of siliceous MFI-type zeolite (silicalite) at various temperatures, to investigate its thermal behavior including the phase transition. Through detailed comparisons between calculated and experimental properties, it was possible to check the validity of our potential model for such a compound and to approach more realistic features of zeolites. This study will also provide a basis for the future study of zeolites with various structures and compositions.

2. Interatomic Potential Model

Interatomic potential functions consist of Coulombic, short range repulsion, van der Waals attraction, and Morse potential terms applied only to the interactions between silicon and oxygen.

$$u_{ij}(r_{ij})=z_i z_j e^2/r_{ij}+f_0(b_i+b_j)\exp[(a_i+a_j-r_{ij})/(b_i+b_j)]-c_{ij}/r_{ij}^6 \quad (3.1)$$
$$+D_{ij}\{\exp[-2b_{ij}(r_{ij}-r^*_{ij})]-2\exp[-b_{ij}(r_{ij}-r^*_{ij})]\}$$

where r_{ij} is an interatomic distance and f_0 (=6.9511×10^{-11}N) is a constant. Parameters, z, a, b and c, are for atomic species, and D_{ij}, B_{ij} and r^*_{ij} are for Si-O pairs. These parameters, which were originally determined using the MD simulations of various silica crystal structures such as quartz, cristobalite, stishovite, etc. [14], were slightly modified for zeolite structures using MD simulations on ZSM-11. All the parameters are listed in Table 3.1.

3. Molecular Dynamics Simulations

MD simulations were carried out using the MD program MXDTRICL [15]. The Ewald method was applied for the summations of Coulombic interactions. The equations of motions were integrated by means of Verlet's algorithm. The temperatures and the pressure were controlled by scaling particle velocities and simulation cell lengths, respectively. In this study, the temperature was varied over the range of 100-1000 K, and the pressure was controlled at 1 atm throughout the MD simulations. The simulation cell corresponds to two crystal unit cells superimposed along c, containing 576 atoms (192 Si and 384 O). Another system of 2304 atoms (768 Si and 1536 O), corresponding to an array of 2 × 2 × 3 unit cells, is applied to examine the relation between thermal expansion and Si-O bonding for the purpose of the average of the larger-scale ensemble. Periodic boundary conditions were adopted. Simulations were started from one of the experimental structures which have orthorhombic or monoclinic symmetry, called ORTHO and MONO respectively by Koningsveld et al. [1,2]. Hereafter we also call the experimental structures ORTHO and MONO. Initial simulations were performed to relax the system for a 5000 steps at 350 K for ORTHO and at 100 K for MONO, with a time step of 0.1 fs (0.1×10^{-15} s). Other runs were always performed with a time step of 2.0 fs (2.0×10^{-15} s). When the temperature was varied, the system was equilibrated by 5000 steps run for the small system and by 20000 steps run for the large one. After the equilibration, a production run of 5000 steps was performed for the small system and that of 20000 steps was done for the large one, and then various time averaged properties were evaluated. Vibrational spectra were calculated from an additional run of 6000 steps for the small system.

4. Results and Discussion

4.1 Vibrational Spectra

The calculated and experimental [16] vibrational spectra are shown in Fig. 3.1. The vibrational spectra were computed as the Fourier transform of the velocity autocorrelation functions of atoms. The calculated vibrational bands are in reasonable agreement with experimental results. This suggests that the oscillatory motion of the framework atoms in the MD simulation is essentially similar to the experimental one.

4.2 Crystal Structures

In order to check the ability of our model to reproduce the orthorhombic and monoclinic phases, MD simulations starting from experimental structures, ORTHO and MONO, were performed at 350 K and at 100 K, respectively. The simulated and experimental lattice parameters are listed in Table 3.2. The molar volume of the simulation at 100 K seems to be slightly contracted relative to that of MONO, because the temperature of the simulation is lower than that of the experimental measurement of MONO. Lattice parameters obtained from the simulation at 350 K show excellent agreement with those of ORTHO. Thus the lattice parameters of these phases are well reproduced by the MD simulations.

Figure 3.2 shows atomic trajectories viewed onto [010] in these MD simulations. The atomic trajectories of the simulation starting from ORTHO are close to atomic positions determined by the X-ray diffraction. The atomic trajectories of the simulation starting from MONO seem to be slightly displaced from experimental positions. The averaged structure of the simulation starting from ORTHO keeps the original orthorhombic *Pnma* symmetry, while that of the simulation starting from MONO changes its symmetry from the original monoclinic $P2_1/n$ to monoclinic *Pn*. Thus the orthorhombic structure is well reproduced by MD simulations with respect to lattice parameters, atomic positions, and a space group symmetry, while the monoclinic

structure of the MD simulation shows a different symmetry from the experimental one. Nevertheless its lattice parameters are in reasonable agreement with experiment. In the next section, we will discuss this in more detail.

4.3 Thermal Behavior

MD simulations over the temperature range of 100-1000 K were carried out. Because both the MD simulations starting from ORTHO and MONO give essentially the same results throughout the temperature range, the following data are represented by those of MD simulations starting from ORTHO. Figure 3.3 shows the time averaged temperature dependence of cell parameters and a molar volume. Cell angles (especially angle α) show orthorhombic angles at high temperature and monoclinic angles at low temperature. In the temperature range of 225-275 K, a drastic change in the α angle occurs. It should be noted that in this temperature range, the angle α fluctuates between ca. 90° and ca. 90.6° as shown in Fig. 3.4. The same results are also obtained from the simulation starting from MONO. The present MD-derived system thus shows the reversible phase transition similar to the experimentally observed one, with respect to the lattice shapes.

The averaged structure has an orthorhombic *Pnma* symmetry above the transition temperature, and a monoclinic *Pn* symmetry below, in agreement with the results of Sec. 4.2. For the monoclinic phase, a cooperative atomic displacement is found in the atomic trajectories at 250 K in Fig. 3.5. This displacement is observed as a jump in the mean square displacement (MSD) of atoms as a function of time as shown in Fig. 3.6. Time averaged structures in three stages presented in this figure are examined with respect to space group symmetry. The results shown in Table 3.3 indicate that the averaged structure in the stage III (equally including time before and after the displacement) has almost the $P2_1/n$ symmetry, while those in the stages I and II (before and after the displacement) have the *Pn* symmetry. Namely, there are two *Pn* configurations for the monoclinic phase, and the average structure of them has $P2_1/n$ symmetry. Our MD

simulations suggest that the experimentally reported monoclinic $P2_1/n$ symmetry can be observed by averaging the two *Pn* configurations over time and space, and another phase with the monoclinic *Pn* symmetry may exists at the lower temperatures. Since most experimental investigations have only been carried out near the transition temperature or at a higher temperature, experimental structural analyses at much lower temperature are desirable.

Table 3.4 shows the thermal expansion coefficient of each phase estimated from slopes of the curve of Fig. 3.3(c). A small change of the thermal expansion is found on the monoclinic-orthorhombic phase transition; the thermal expansion coefficient above the transition temperature is smaller than that below the transition temperature. This difference has not been confirmed by experimental measurements.

As temperature increases further, the thermal expansion coefficient shows another remarkable change and becomes negative at 450 K, while the space symmetry remains the same. It is known from experimental measurements [17], as well as by MD simulations, that quartz and cristobalite, analogous to zeolites, change into a higher-temperature phase with nearly zero or negative values of thermal expansion coefficients. Our MD simulations, therefore, suggest that the zeolite may show a phase transition to a higher-temperature phase similar to what analogs.

4.4 Relation between Thermal Expansion and Si-O Bonding

The temperature dependence of Si-O bonding is examined by the MD simulation of the large system of 2304 atoms (768 Si and 1536 O). In Fig. 3.7, the monoclinic lattice changes into an orthorhombic one at 240 K, and the thermal expansion coefficient becomes almost zero at the temperatures higher than 500 K. The thermal behaviour of the large system is, thus, consistent with that of the small system. The temperature dependence of bonding structure is shown in Fig. 3.8. The average Si-O distance monotonously increases with temperature, while the others drastically increase during the phase transition and the slopes of both curves change at 400 K. The average Si-O-Si

angle increases to 400 K with temperature. This as well as the expansion of the Si-O distance results in the positive thermal expansion of the Si-Si distance. At the temperatures higher than 400 K, the Si-O-Si angle decreases with temperature so that the Si-Si distance varies little by the offset of the expansion of the Si-O distance. It is also shown in Figs. 3.7 and 3.8 that the temperature dependence of the Si-Si distance agrees approximately with that of molar volume.

It becomes clear that the nearly zero or negative values of thermal expansion coefficient at the higher temperature for the orthorhombic phase is related to the decrease in the Si-O-Si angle with increasing temperature, like the case of β-cristobalite discussed in Chapter 2. The negative temperature dependence of the Si-O-Si angle is attributed to the great freedom of transverse oxygen vibrations because of the openness of the structure. Namely, an oxygen atom is distributed over a circle centered on the Si-Si line, and the radius of the circle increases with temperature, which means the decrease in the average Si-O-Si angle. On the other hand, the very low thermal expansion is not observed right above the phase transition temperature but at the temperatures higher than 400 K, differently from the case of cristobalite. It should be noted here that the phase transition temperature of 230 K for the MFI-type zeolite is lower than that of 450 K for cristobalite, as well as the average Si-O-Si angle of 155.6° after the phase transition is smaller than that of 165.4° for cristobalite. This suggests that the effect of transverse oxygen vibration on the Si-O-Si angle is considerable at higher temperature and wider Si-O-Si angle.

5. Conclusion

MD simulations of MFI-type zeolite reproduce well the orthorhombic structure above the transition temperature and the monoclinic lattice below the transition temperature. The phase transition similar to the experimentally observed one takes place in the range 225-275K. The vibrational spectra are also in reasonable agreement with the experimental ones. Thus our MD simulations successfully reproduce some characteristics of the zeolite. This indicates that the potential model used here is sufficiently appropriate for molecular simulations of this type of zeolites. Considering that the potential model was slightly modified from that originally adopted for silica polymorphs except for zeolites, it is expected that the present potential model will be widely effective on silica compounds including zeolites.

In the MD simulations, the low temperature monoclinic phase shows *Pn* symmetry instead of the experimentally reported $P2_1/n$ symmetry. In addition, a cooperative atomic displacement between two monoclinic *Pn* configurations is found at 250 K. The average structure of the two *Pn* configurations almost show the $P2_1/n$ symmetry. Thus the MD simulations suggest the existence of monoclinic *Pn* phase as well as the experimental $P2_1/n$ phase. It is also found that the thermal expansion becomes negative or nearly zero in the higher temperature range (>500 K). This suggests the existence of a higher-temperature phase similar to that observed for β-quartz and β-cristobalite. In te temperature range simulated, the thermal expansion of this zeolite almost corresponds to the variation in the Si-Si distance, and the very low thermal expansion is ascribed to the decrease in the Si-O-Si angle. Finally, the relation of those phases obtained from the MD simulations for the MFI-type zeolite is schematically illustrated in Fig. 3.9.

References

[1] H. van Koningsveld, J.C. Jansen, and H.van Bekkum, Zeolites, **10** (1990) 235.

[2] H. van Koningsveld, Acta Cryst, **B46** (1990) 731.

[3] A. Lopez, M.Soulard and J. L. Guth, Zeolites, 10 (1990) 134.

[4] H. van Koningsveld, J. C. Jansen, and H. van Bekkum, Zeolites, **9** (1987) 243.

[5] H. Strobl, C.A. Fyfe, G.T. Kokotailo, and C.T. Pasztor, J. Am. Chem. Soc., **109**, (1987) 4733.

[6] E.L. Wu, S.L. Lawton, D.H. Olson, A.C. Rohrman, Jr., and G.T. Kokotailo, J. Phys. Chem., **83**, 21, (1979) 2777.

[7] C.A. Fyfe, H. Strobl, G.T. Kokotailo, G.J. Kennedy, and G.E.Barlow, J. Am. Chem. Soc., **110** (1988) 3373.

[8] C.A. Fyfe, H. Grondey, Y, Feng, and G.T. Kokotailo, J. Am. Chem. Soc., **112** (1990) 8812.

[9] H. Lermer, M. Draeger, J. Steffen, and K.K. Unger, Zeolites, **5** (1985) 131.

[10] D. H. Olson, G.T. Kokotailo, S.L. Lawton, and W.M. Meler, J. Phys. Chem., **85** (1981) 2238.

[11] R.G.Bell, R.A.Jackson, and C.R.A.Catlow, J. Chem. Soc., Chem. Commun, (1990) 782.

[12] E.de Vos Burchart, H.van Bekkum, and B.van de Graaf, Zeolites, **13** (1993) 212.

[13] P.Demontis, G.B. Suffritti, S. Quartieri, A. Gamba, and E. S. Fois, J. Chem. Soc. Faraday Trans., **87** (1991) 1657.

[14] K.Kawamura, in: Molecular Dynamics Simulations, ed. F.Yonezawa, (Springer-Verlag, 1990) p.88.

[15] K. Kawamura, MXDTRICL, Japan Chemistry Program Exchange, #077; K.Kawamura, JCPE Newsletter, **5**(2) (1993) 30.

[16] D. Scarano, A.Zecchina, S. Bordiga, F. Geobaldo, G. Spoto, G. Petrini, G. Leofanti, M. Padovan, and G. Tozzola, J. Chem. Soc. Faraday Trans., **89**, 22 (1993) 4123.

[17] R.J. Ackermann and C.A. Sorrell, J. Appl. Cryst., **7**, (1974) 461.

Table 3.1. Parameters of interatomic potential model.

Ion	z	a (Å)	b (Å)	c ($kJ^{1/2}$ Å $^3mol^{-1/2}$)
O	-1.2	1.905	0.150	40.9
Si	2.4	0.935	0.100	0.0

Ion pair	D (10^{-19} J)	β	r^* (Å)
Si-O	5.63	2.00	1.51

Table 3.2. Crystal structures obtained from experiments and simulations.

	a (Å)	b (Å)	c (Å)	α (°)	β (°)	γ (°)	ρ (g/cm^3)
ORTHO[a]	20.08	19.90	13.37	90	90	90	1.793
MONO[b]	20.11	19.88	13.37	90.67	90	90	1.792
Simulation from ORTHO at 350 K	20.08(5)	19.89(5)	13.46(2)	89.97(9)	90.01(9)	90.02(5)	1.781(7)
Simulation from MONO at 100 K	19.94(2)	19.72(2)	13.41(1)	90.68(3)	90.00(3)	90.00(2)	1.817(3)

[a]Experimental orthorhombic structure at 350 K.

[b]Experimental monoclinic structure at room temperature.

Table 3.3. Mean-deviation from coordinates of two space groups (Unit: Å).

Symmetry	I[a]		II[a]		III[ab]	
	O	Si	O	Si	O	Si
$P2_1/n$	0.208	0.174	0.226	0.191	0.0412	0.0324
Pn	0.0075	0.00767	0.0102	0.0091	0.0084	0.0069

[a]Symbols, I, II and III, represent the stages indicated in Fig. 3.6.

[b]Note that Pn symmetry is a subgroup of $P2_1/n$ one. Therefore, the mean-deviations concerning both the two groups become small if coordinates have $P2_1/n$ symmetry.

Table 3.4. Calculated thermal expansion coefficients.

Initial structure	Monoclinic-phase (K^{-1})	Orthorhombic-phase (K^{-1})	HT-Orthorhombic-phase (K^{-1})
ORTHO	5.7×10^{-5}	4.4×10^{-5}	-2.3×10^{-6}
MONO	5.2×10^{-5}	4.3×10^{-5}	-4.9×10^{-6}

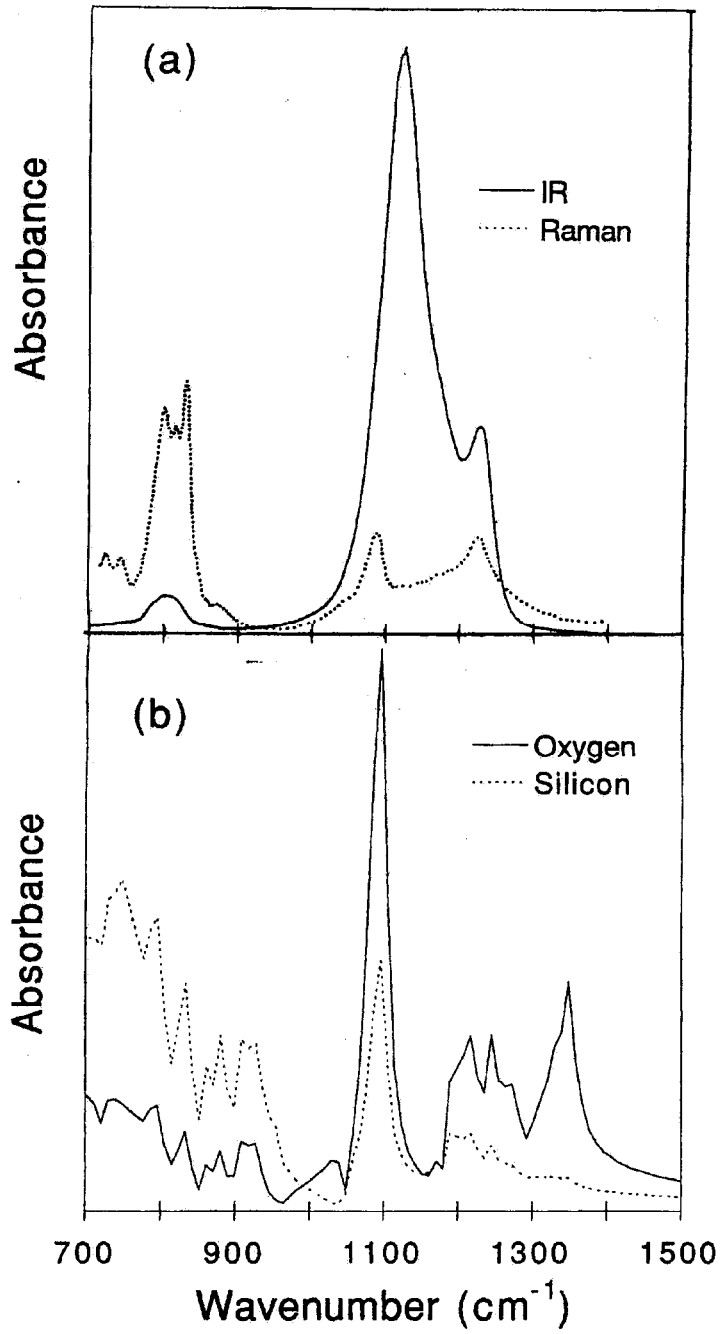

Fig. 3.1 Vibrational spectra of silicalite; The experiment at room temperature (a) [16] and the simulation at 350K (b).

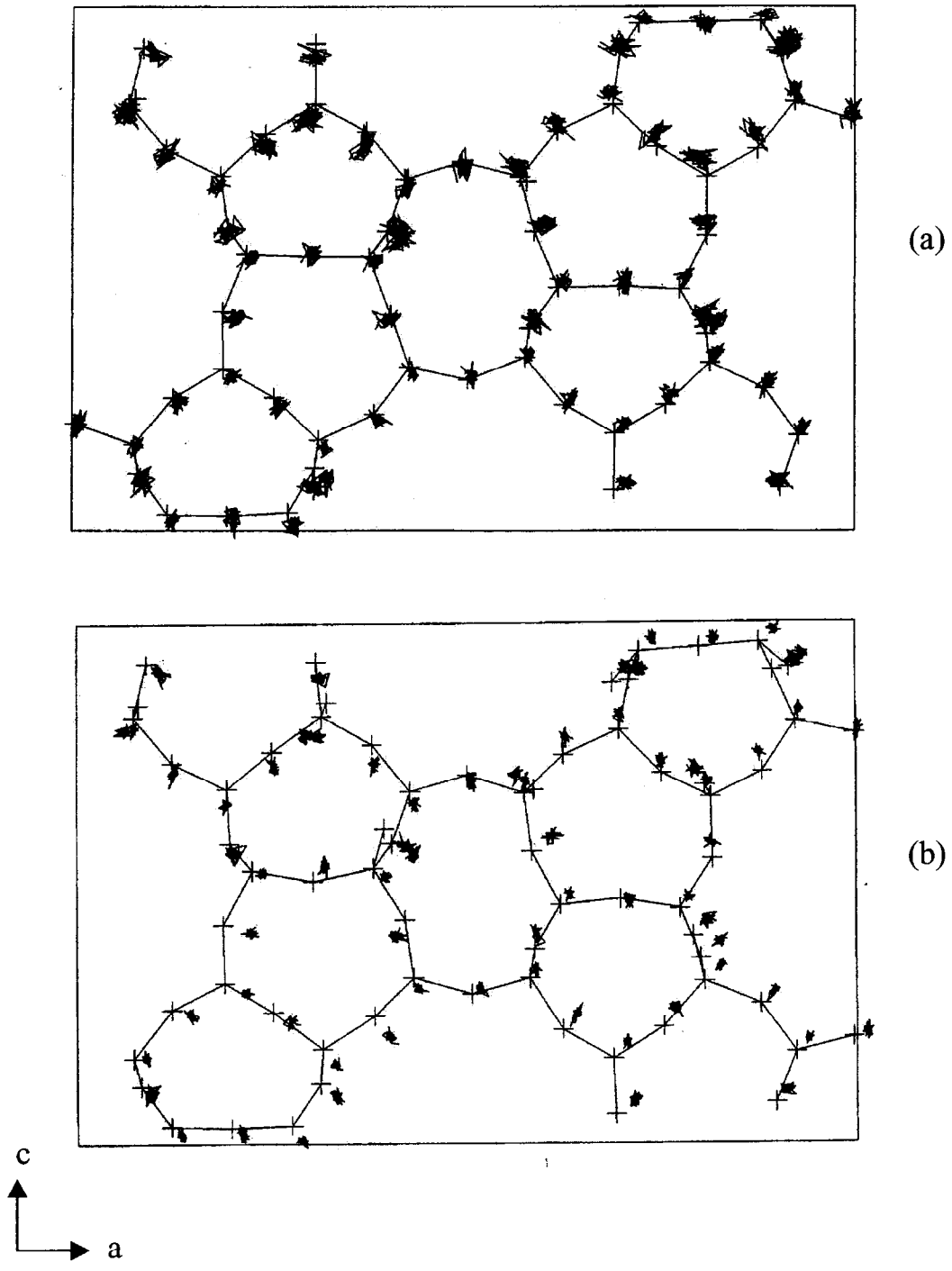

Fig. 3.2 Atomic trajectories viewed onto [010]; The simulation starting from ORTHO at 350 K (a), and from MONO at 100 K (b). The depth along b axis corresponds to fifth of b length of a crystal unit cell. Crosses represent the atomic positions determined by experimental measurements at 350 K for ORTHO and at room temperature for MONO.

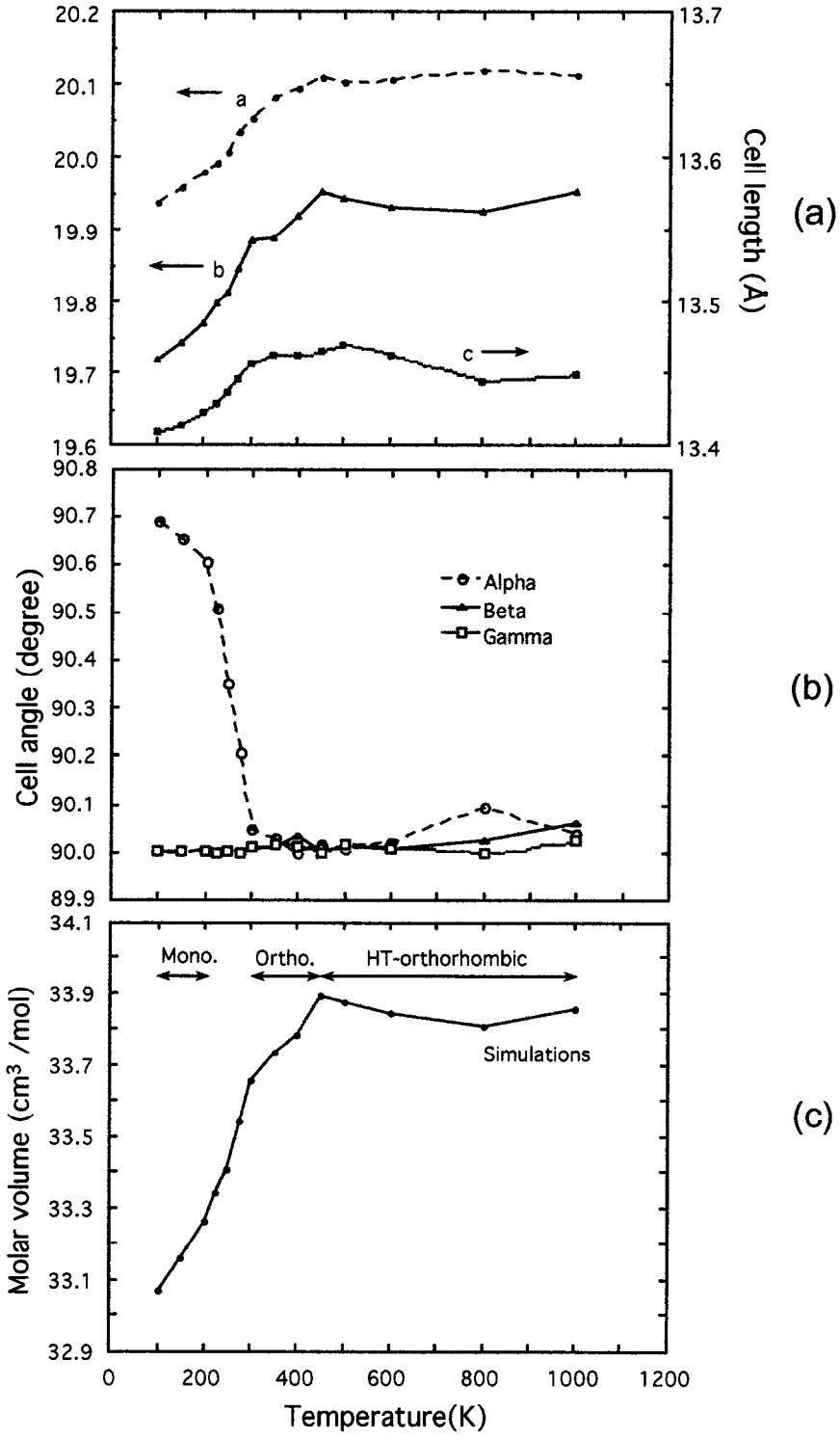

Fig. 3.3 Temperature dependence of cell parameters (a) (b) and molar volume (c) obtained from the simulation starting from ORTHO.

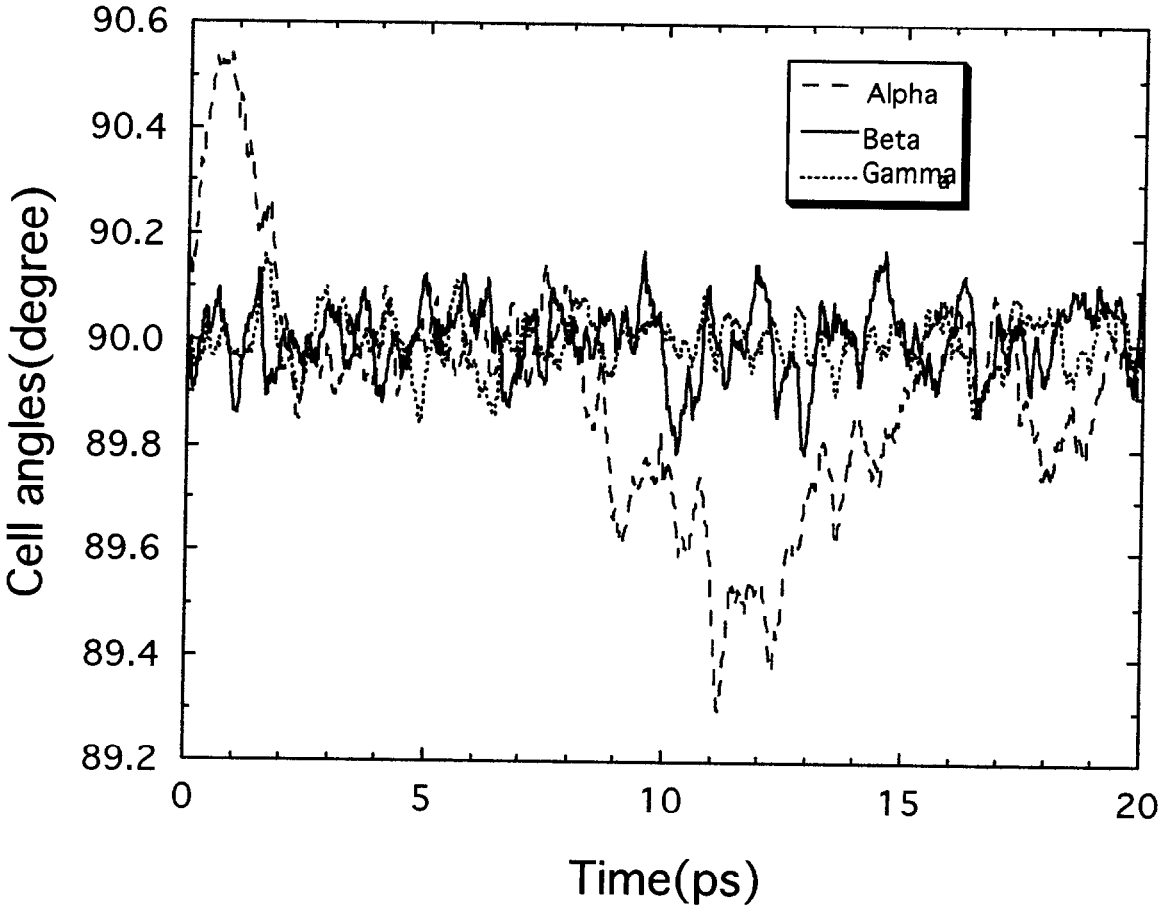

Fig. 3.4 Cell angle variations obtained from the simulation at 275 K.

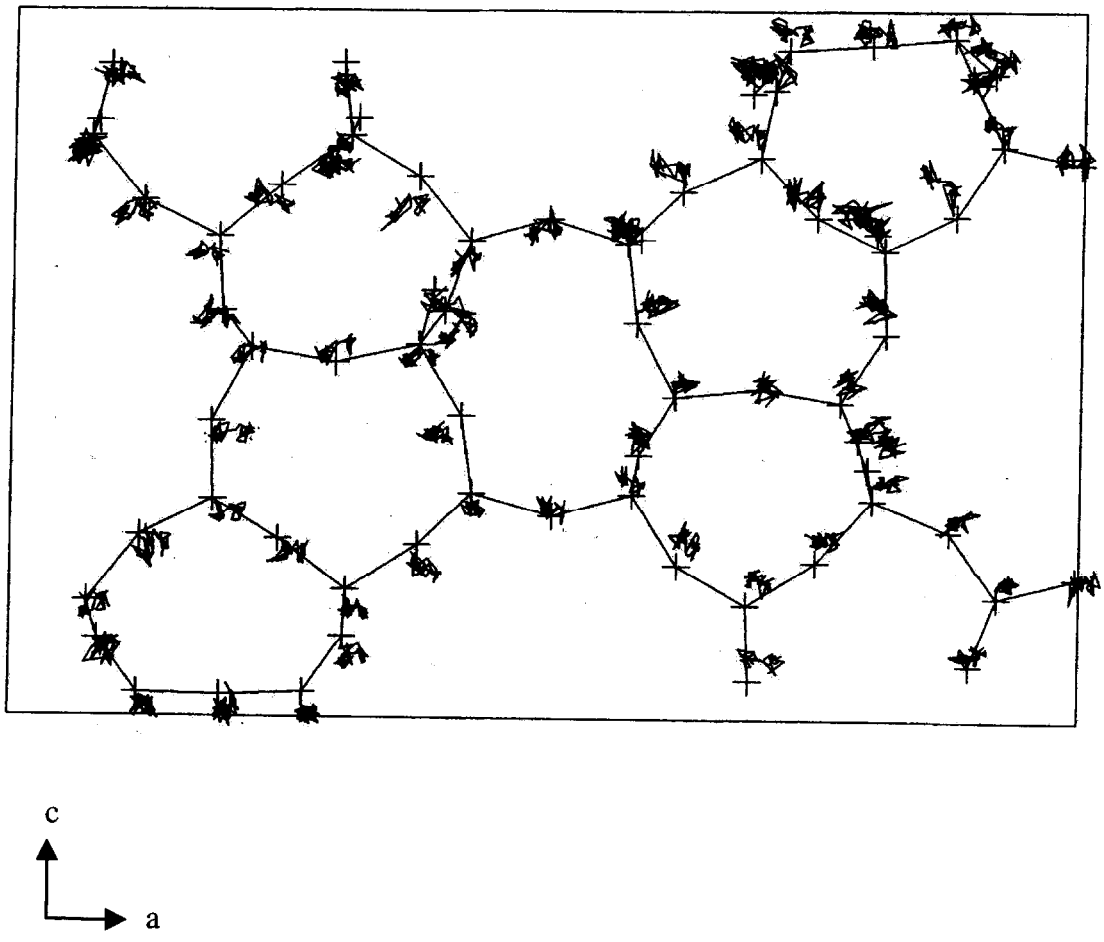

Fig. 3. 5 Atomic trajectories viewed onto [010] at 250 K. The depth along b axis corresponds to fifth of b length of a crystal unit cell. Crosses represent the atomic positions determined by experimental measurements at room temperature for MONO.

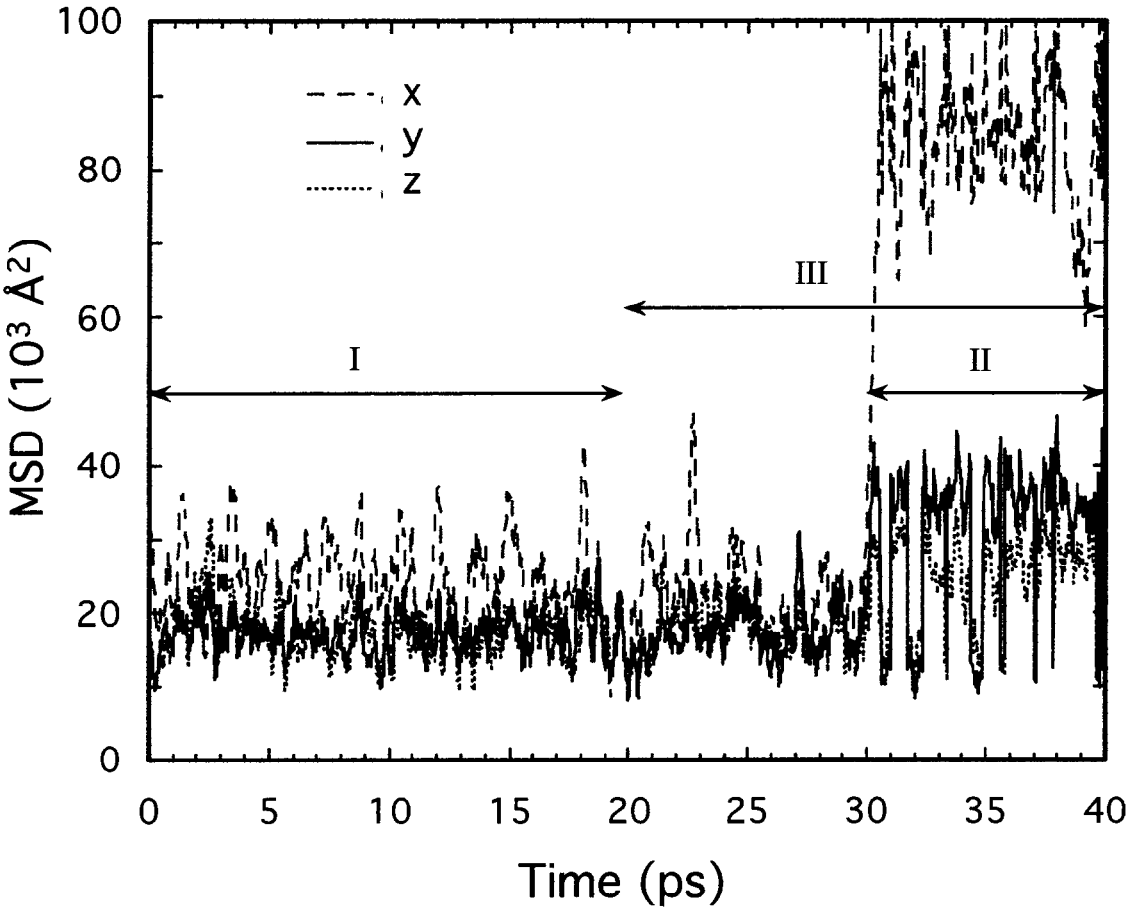

Fig. 3.6 Mean-square displacements of oxygen atoms at 250 K. The simulated structure keeps monoclinic. The stages I and II represent the time before and after the displacement, respectively. The stage III equally includes the time before and after the displacement.

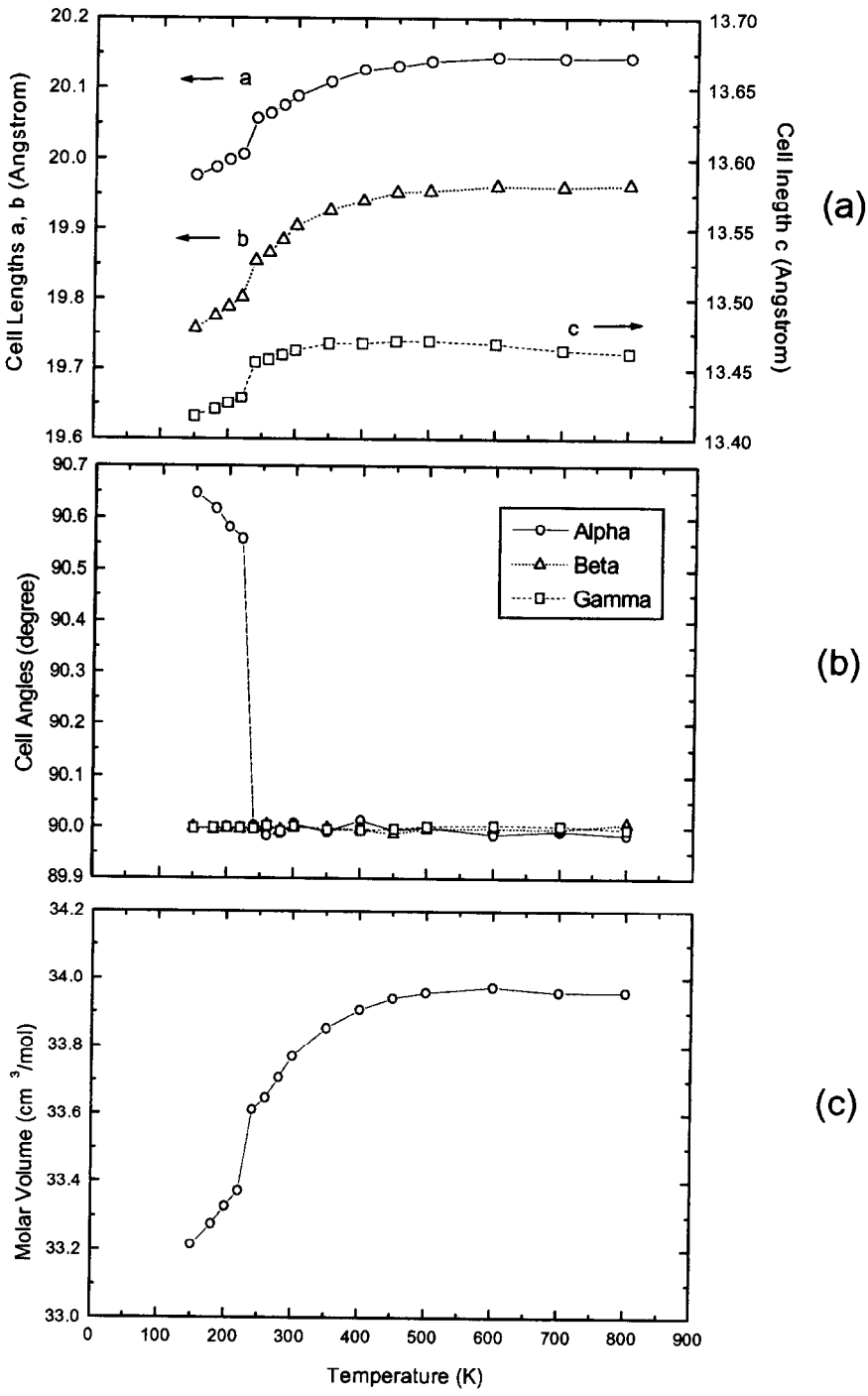

Fig. 3. 7 Temperature dependence of cell parameters (a) (b) and molar volume (c) obtained from the simulation for the large system of 2304 atoms (768 Si and 1536 O) starting from ORTHO.

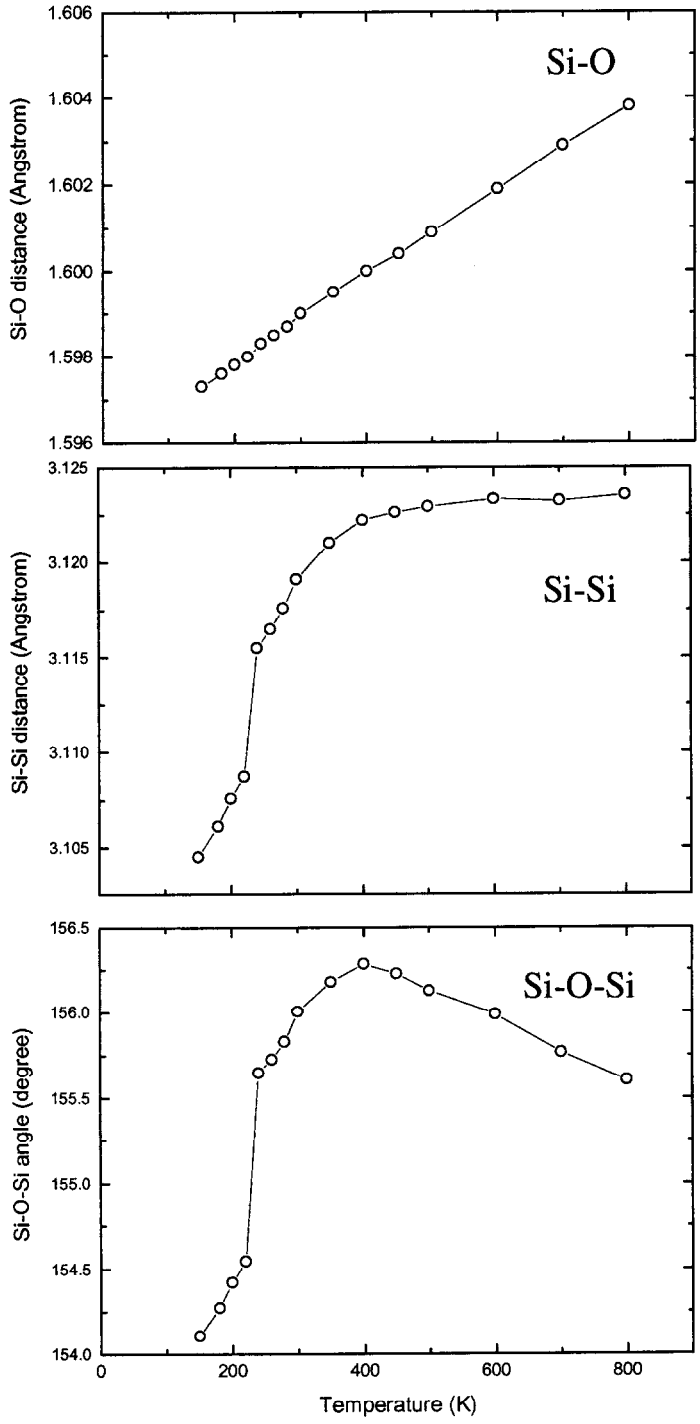

Fig. 3. 8 Temperature dependence of microstructure parameters (a) Si-O distance, (b) Si-Si distance, and (c) Si-O-Si angle obtained from the simulation for the large system of 2304 atoms (768 Si and 1536 O) starting from ORTHO.

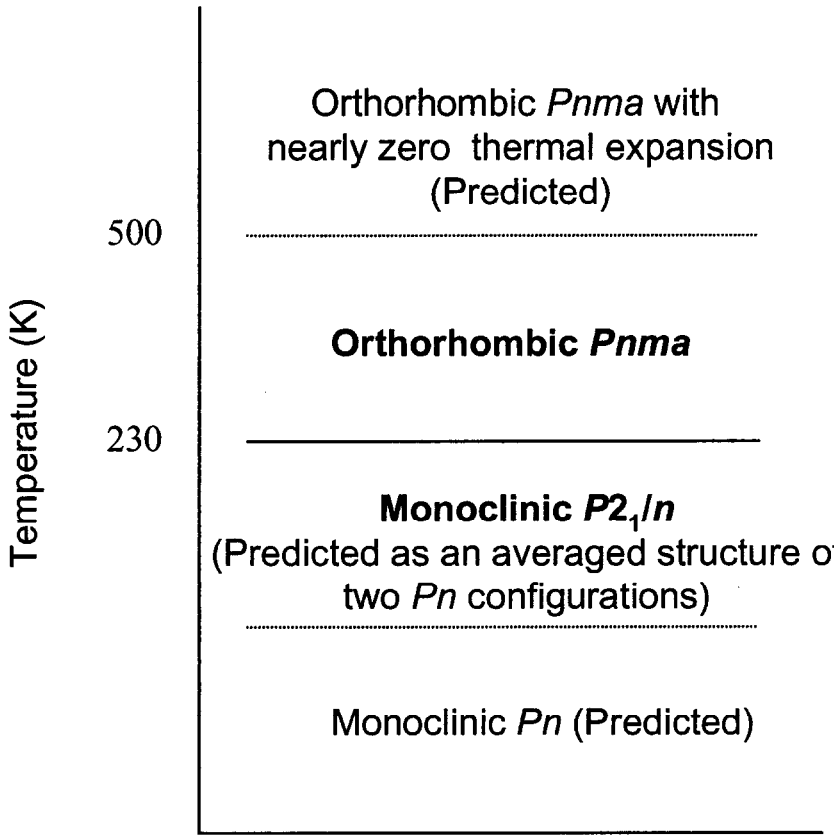

Fig. 3. 9 Schematic diagram of phase relation obtained from the MD simulations for the MFI type zeolite. Bold letters represent the experimentally reported phases.

Chapter 4

Structural Development in Sol-Gel Process for Silica Systems

1. Introduction

The sol-gel process is an important method for producing various commercial silica gels such as fibers, coating films, adsorbents, and catalyst supports. Typically, alkoxysiloxanes are used as the silica source. There are the hydrolysis and condensation reactions proceeding concurrently, which have been studied in detail [1]. Such polymerization process consists of the following three functional group reactions:

$$\text{SiOR} + \text{H}_2\text{O} \xrightarrow{k_h} \text{SiOH} + \text{ROH} \quad (4.1)$$

$$2\text{SiOH} \xrightarrow{k_{cw}/2} 2(\text{SiO})\text{Si} + \text{H2O} \quad (4.2)$$

$$\text{SiOR} + \text{SiOH} \xrightarrow{k_{ca}/2} 2(\text{SiO})\text{Si} + \text{ROH} \quad (4.3)$$

where k_h, k_{cw} and k_{ca} are the rate constants of hydrolysis and water- and alcohol-producing condensations, respectively. The optical and physical properties of product gels strongly depend on the conditions of reaction such as initial composition, temperature and pH through the three-dimentional network structures obtained. However, the details of the structural development in gel formation process are not yet well understood.

Assink and Kay [2,3] and Kay and Assink [4] proposed a new statistical model using the experimentally determined values of k_h, k_{cw} and k_{ca} to calculate both the equilibrium distribution of Si species as a function of H_2O/Si ratio and the time evolution during acid-catalyzed hydrolysis for tetramethoxyorthosilicate (TMOS). Here, the Si species, $Si(OR)_X(OH)_Y(OSi)_Z$, are characterized by the functional groups of the nearest neighbor. The hydrolysis and condensation reactions were successfully described by the model. This suggests that steric and electronically inductive effects as well as reverse reactions such as re-esterification are not important for the early stage of

hydrolysis and condensation of TMOS at the low amount of water, because the statistical model ignores these factors.

Garofalini and Martin [5] first applied MD simulation to a sol-gel process for a silica system to understand the mechanism of the condensation process. The simulation results for silicic acid were consistent with experimental data of sol-gel systems. The formation of linear and branched chains at the early stage of polymerization was followed by ring formation. This conformed well to the interpretation from the NMR data and the semiempirical molecular orbital calculations. The calculated activation energy of formation for branched Q_n species was consistent with that obtained experimentally for gelation. Here, the Q_n species are defined by the number n of bridging oxygen around the Si atom. The relative changes of composition for Q_n species with time were in agreement with the experimental NMR data. Furthermore, the condensation polymerization was seen to depend on the existence of non-bridging oxygen coordinated with hydrogen, the number of bridging oxygen around the five-coordinated Si atom and the atomic momentum created as molecules approach each other [6].

In the present study, we investigated the atomistic features of structural development using MD simulation for two characteristic systems: silicic acid, $Si(OH)_4$, and monomethoxy silicic acid, $Si(OMe)(OH)_3$. Hereafter the former is called THS (tetrahydroxysilane) and the latter MMS. The two systems were regarded as differing from each other in the extent of hydrolysis. The simulation results were compared with the ^{1}H-NMR data reported by Kay and Assink [4], in terms of the Q_n species distribution as a function of SiOSi/Si ratio. Moreover, maximum cluster size, cluster type, ring size distribution, and network structure were examined to make clear the characteristic of polymerization process. The effect of the remaining methoxy groups on the structural development was also found from a detailed comparison of the simulation results for both systems.

2. Interatomic Potential Model

The interatomic potential employed was the same as that used in the similar simulation by Fueston and Garofalini [7] except an additional term for Me-O bond. The interatomic potential contains a two-body term and a three-body term. The former term has a short-range repulsion and a screened Coulomb for all atom pairs, and a specific term for all pairs involving hydrogen atoms. The latter term confines each bond angle to the equilibrium value. The potential is given below:

$$U_{ij}(r_{ij}) = A_{ij}\exp(-r_{ij}/\rho_{ij}) + Z_i Z_j e^2/r_{ij}\, erfc(r_{ij}/\beta_{ij}) \tag{4.4}$$

$$U_{jik}(r_{ij}, r_{ik}, \theta_{jik}) = \lambda_{jik}\exp[\gamma_{ij}/(r_{ij}-r^0_{ij}) + \gamma_{ik}/(r_{ik}-r^0_{ik})] \times(\cos\theta_{jik}-\cos\theta^0_{jik})^2,$$

$$\text{if } r_{ij}<r^0_{ij} \text{ or } r_{ik}<r^0_{ik} \tag{4.5a}$$

$$U_{jik}(r_{ij}, r_{ik}, \theta_{jik}) = 0, \text{ if } r_{ij}>r^0_{ij} \text{ or } r_{ik}>r^0_{ik} \tag{4.6b}$$

$$U_H = a_{ij}/\{1 + \exp(b_{ij}(r_{ij}-c_{ij}))\}, \text{ for Si-H, O-H and H-H} \tag{4.7}$$

where Z_i and Z_j are the formal ionic charges on atoms i and j, e the elementary electric charge, r_{ij} the interatomic distance, θ_{jik} the angle between bonds ij and ik, and A, ρ, β, a, b, c, r^0 and θ^0 are the empirical parameters. In addition, for the system of MMS an extra term was included in the potential to account for the existence of the stable Me-O bond, which is not broken in the sol-gel process. We paid much attention to the effect of the remaining methoxy groups on the structural development and the gel structure. For this purpose a harmonic term with a large force constant was introduced:

$$U_{Me} = 1/2K(r_{ij}-r^0)^2, \text{ for Me-O} \tag{4.8}$$

where K is the harmonic force constant, r^0 the equilibrium length. Methyl groups were treated as united atoms. It is not always necessary that various potential parameters associated with methoxy groups are determined exactly. In fact, several MD simulations using different parameter sets associated with methoxy groups, where the

polymerization reaction occurred, gave common characteristic features as described later. The charge of a methyl group attached to non-bridging oxygen strongly influenced the progress of polymerization. In this paper, the simulation results using a typical parameter set will be presented for MMS. These two and three body potential parameters are listed in Tables 4.1 and 4.2.

3. Molecular Dynamics Simulations

MD simulations were carried out using the MD program MXDORTO developed by Kawamura [8]. The equations of motion were integrated by means of a Verlet's algorithm. The time step used in MD runs was 0.4 fs. The systems composed of 216 molecules were simulated for THS and MMS. Densities were varied from 1.40 to 1.60 g/cm^3 for THS and from 1.83 to 2.20 g/cm^3 for MMS. We confirmed the density independence of the relative remarkable difference between THS and MMS in the structural development and the gel structure. The simulation results with densities of 1.60 (THS) and 1.83 g/cm^3 (MMS) will be presented later. This results in a periodic cubic cell with a length of 27.6 Å on a side. After the molecules were distributed randomly at 500 K, polymerization runs of 4×10^5 time steps were performed at 2500 K. Temperature was controlled by scaling particle velocities. The high density and high temperature conditions were adopted to accelerate polymerization and reduce computation time drastically, following the similar approach by Garofalini and Martin [5].

4. Results and Discussion

Atomistic features of the structural development are discussed through Q_n species distribution, number of siloxane bonds per Si atom (SiOSi/Si ratio), maximum cluster size, cluster type, ring size distribution and network structure. Here, chemical bonds were judged by the interatomic distances whose thresholds are 2.2, 1.6 and 1.5 Å for Si-O, Me-O, and O-H bonds, respectively. Ring size distribution was analyzed using CATALYSIS Ver. 5.0 [9] developed by Molecular Simulations Inc.

4.1. Comparison of Q_n Species Distribution between MD Simulation and ^{1}H-NMR

Fig. 4.1 shows the calculated Q_n species distribution as a function of SiOSi/Si ratio for THS with that determined experimentally using ^{1}H-NMR [4]. The latter is the equilibrium distribution of Q_n species for various initial H_2O/Si ratios. The initial H_2O/Si ratio is almost equal to the SiOSi/Si ratio at long reaction time for low H_2O/Si ratios, where the hydrolysis of siloxane bonds can be neglected. Q_4 species containing no hydrogen is not detected by ^{1}H-NMR. The content of both Q_5 and Q_6 species in the MD simulations under high temperature and pressure is below 6% of the total amount of Q_n species. The calculated Q_n species distribution is in good agreement with that from the experiment at the SiOSi/Si ratios below 0.8. At the larger SiOSi/Si ratios, the calculated compositions of Q_2 and Q_3 species tend to be smaller than the experimental data, and the trend for Q_0 is the opposite. This behavior would be attributable to hydrolysis of siloxane bonds as mentioned above. It is quite difficult to compare directly the Q_n species distribution as a function of time between MD simulation and experiment, because the time scale of MD simulation is some orders of magnitude less than that of experiment. Instead of this, MD simulation reproduced well the corresponding experimental Q_n species distribution as a function of SiOSi/Si ratio at the low ratios.

4.2. SiOSi/Si ratio and Q_n Species Distribution

The time evolution of the calculated SiOSi/Si ratio for THS and MMS is shown in Fig. 4.2. There is almost no difference at the early stage. The difference between them is found at the intermediate and final stages. This behavior can be understood from the comparison of time evolution of Q_n species distribution as shown in Fig. 4.3. The formation of siloxane bonds is nearly dominated by the situation of Q_1 and Q_2 species at the initial stage. The formation rates in both systems are not so different. Since then, the existence of Q_3 and Q_4 species becomes significant. The formation rates for MMS are slightly smaller than those for THS. This indicates that a methoxy group remaining on a Si atom mainly interferes with the formation of Q_3 and Q_4 species.

4.3. Maximum Cluster Size

Fig. 4.4 shows the time evolution of maximum cluster size represented by the number of Si atoms constituting the cluster. The maximum cluster size increases slowly at the early stage and rapidly to a half of the total amount of Si atoms around 25 ps and 40 ps for THS and MMS, respectively. These times correspond to the SiOSi/Si ratio of about 0.9. Fig. 4.5 shows the time evolution of number of small clusters, which are divided into three groups by cluster size. A lot of clusters appear and grow stepwise from dimer to larger oligomer at the early stage. When a cluster consisting of about 40 Si atoms is formed as shown in Fig. 4.4, the rapid cluster growth takes place through aggregation of such small clusters. After that until about 60 ps (THS) or 110 ps (MMS), maximum cluster size increases and the number of small clusters decreases gradually with the relatively large fluctuation, on the whole. An enormous cluster of a rough network sometimes decomposes into small clusters. The network, which is linked infinitely in at least one direction by periodic boundary condition, becomes closer, repeating the formation and dissociation of bonds. Here, the maximum cluster size is equal to the number of Si atoms constituting the network in the real simulation cell. In particular, some pronounced features are found for MMS. This also indicates that the

remaining methoxy groups interfere with the cluster-cluster aggregation and the cross-linking process.

4.4. Cluster Type

The clusters are divided into the following types: linear, branched and cyclic. A linear cluster has neither branch nor ring, a branched cluster has no ring, and a cyclic cluster has at least a ring. The calculated number of all types of cluster as a function of time is shown in Fig. 4.6. First, a lot of linear clusters occur. Second, the branched clusters and subsequently the ring clusters arise. The maximum cluster size of linear clusters is less than 10 during polymerization.

4.5. Atomistic Picture of the Structural Development

The calculated ring size distribution curves at different times for THS are shown in Fig. 4.7. Ring sizes are represented by the number of Si atoms composing rings. The corresponding snapshots are presented in Fig. 4.8, with the time evolution of maximum cluster size in Fig. 4.4(a). For a clear description of clusters and gel structure, Si-O bonds attached to bridging oxygen and monomers denote lines and crosses, respectively, where the other atoms and bonds are omitted. Small clusters are observed in the snapshots at 10 ps and 20 ps before the rapid cluster growth. As shown in Fig. 4.6 (a), there are mainly linear and branched clusters around 10 ps, and cyclic clusters appear considerably at 20 ps. These clusters have relatively small rings less than 7-rings as shown in Fig. 4.7. The total number of rings goes on increasing until 160 ps. A silica network over the box space appears on the snapshot of 40 ps owing to cluster-cluster aggregation. The number of 5-rings increases largely. Subsequently, the larger rings from ring size 6 to 8 are added to a great extent at the final stage. In addition, the silica network, which is relatively homogeneous at 40 ps, gradually becomes heterogeneous. Through the repeated bond formation and breaking, the silica network gets denser and separates into a silica-rich phase and a solvent-rich phase slowly with decreasing the

total potential energy. Fig. 4.9 compares the network structures of THS and MMS at 160 ps. The gel structure of THS is denser than that of MMS. It is confirmed that the remaining methoxy groups interfere with constructing dense network structure.

5. Conclusion

Polymerization process yielding gels was studied using molecular dynamics simulations for silicic acid and monomethoxy silicic acid. The calculated Q_n species distribution as a function of SiOSi/Si ratio is in good agreement with that observed by ^{1}H-NMR. Atomistic features of the structural development were extracted from a series of the simulation results. There is a slow cluster growth during the early stage, a rapid cluster growth follows this due to cluster-cluster aggregation, and the network structure becomes denser with time through the repeated bond-formation and bond-breaking. Finally the trend of phase separation is observed. The remaining methoxy group interferes with the aggregation and the formation of the dense network structure. The present simulations performed give a reasonable picture from a microscopic point of view. Having some problems to be examined about set temperature, system size and dilution effect, MD simulation has proved effective for obtaining useful structural information on sol-gel process for silica systems.

Rererences

[1] C. J. Brinker and G. W. Scherer, Sol-Gel Science (Academic Press, San Diego, CA, 1990).

[2] R.A. Assink and B.D. Kay, J. Non-Cryst. Solids, **99** (1988) 359.

[3] B. D. Kay and R. A. Assink, J. Non-Cryst. Solids, **104** (1988) 112.

[4] R.A. Assink and B.D. Kay, J. Non-Cryst. Solids, **107** (1988) 35.

[5] S. H. Garofalini and G. E. Martin, J. Phys. Chem., **98** (1994) 1311.

[6] G. E. Martin and S. H. Garofalini, J. Non-Cryst. Solids, **171** (1994) 68.

[7] B. P. Feuston and S. H. Garofalini, J. Phys. Chem., **94** (1990) 5351.

[8] K. Kawamura, MXDORTO, Japan Chemistry Program Exchange, #029; K. Kawamura, "MXDORTO", JCPE Newsletter, **4**, 3 (1992) 48.

[9] CATALYSIS Ver.5.0, Molecular Simulations, Inc., San Diego, CA, 1996.

Table 4.1 Parameters for the two-body potential in Eqs. (4.4), (4. 6) and (4.7)

	A ($\times 10^{-9}$ erg)	ρ (Å)	β (Å)	a ($\times 10^{-12}$erg)	b (Å^{-1})	c (Å^{-1})	r^0 (Å)	K ($\times 10^{-9}$ erg Å^2)
Si-Si	1.8770	0.29	2.29					
Si-O	2.9620	0.29	2.34					
O-O	0.7250	0.29	2.34					
Si-H	0.0690	0.29	2.3 1	-4.6542	6.0	2.20		
H-H	0.0340	0.35	2.10	-5.2793	6.0	1.5 1		
				+0.3473	2.0	2.42		
O-H	0.3984	0.29	2.26	-2.0840	15.0	1.05		
				+7.6412	3.2	1.50		
				-0.8336	5.0	2.00		
[a]Me-Me	3.000	0.29	2.10					
[a]Me-Si	1.500	0.29	2.10					
[a]Me-O	1.000	0.29	2.10				1.43	1.0
[a]Me-H	0.400	0.29	2.10					

[a]Additional parameters associated with methoxy groups, whose charge is zero.

Table 4.2 Parameters for the three-body potential in Eqs. (4.5a) and (4.5b)

	O-Si-O	Si-O-Si	Si-O-H	H-O-H	[a]Si-O-Me	[a]H-O-Me
λ ($\times 10^{-11}$ erg)	19.0	0.3	5.0	35.0	5.0	35.0
γ(Å)						
Si-O	2.8					
O-Si		2.0	2.0		2.0	
O-H			1.2	1.3		1.2
O-Me					2.0	2.0
r^0 (Å)						
Si-O	3.0					
O-Si		2.6	2.6		2.6	
O-H			1.5	1.6		1.5
O-Me					2.3	2.3
θ^0 (deg.)	109.5	109.5	109.5	104.5	109.5	1 08.0

[a]Additional parameters associated with methoxy groups.

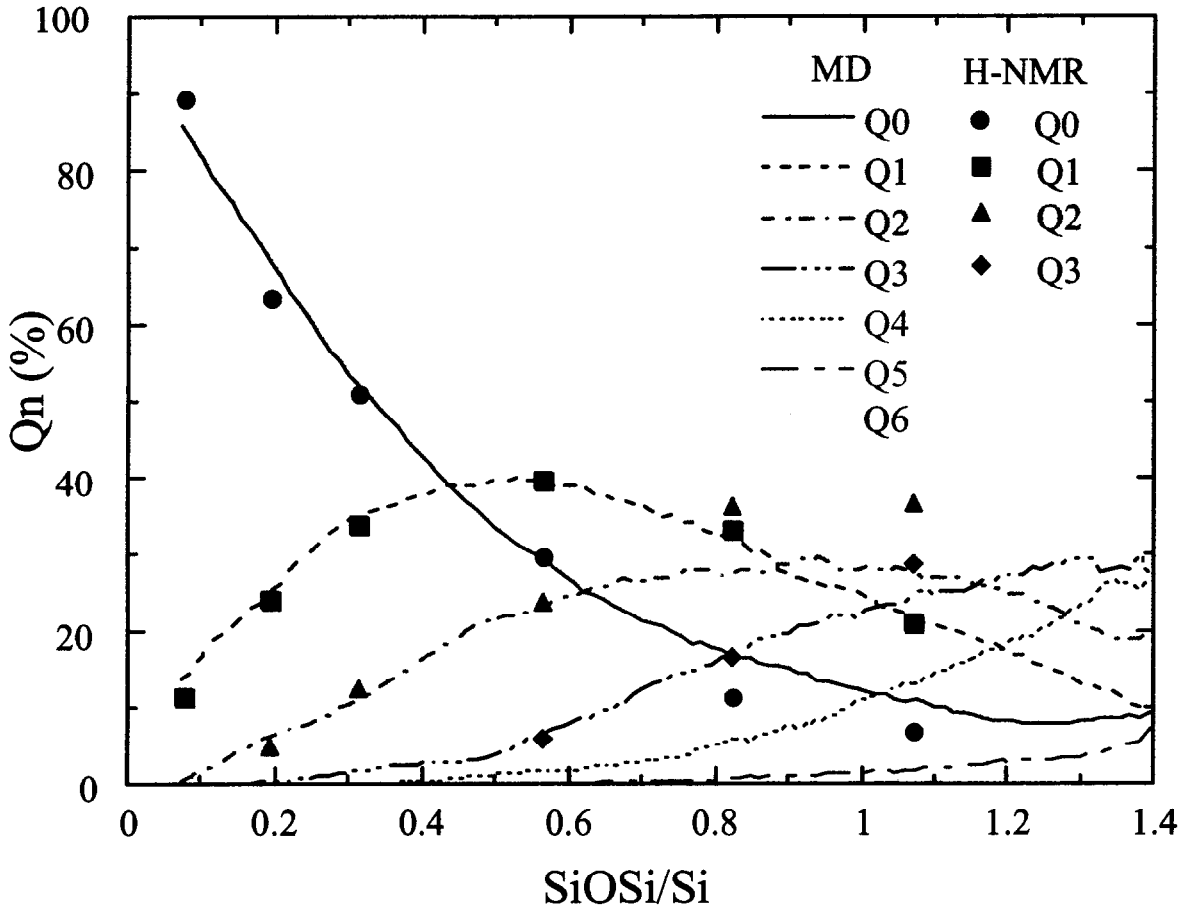

Fig. 4.1 Composition of Q_n species as a function of SiOSi / Si ratio. Data from ^{1}H-NMR and MD simulation for THS.

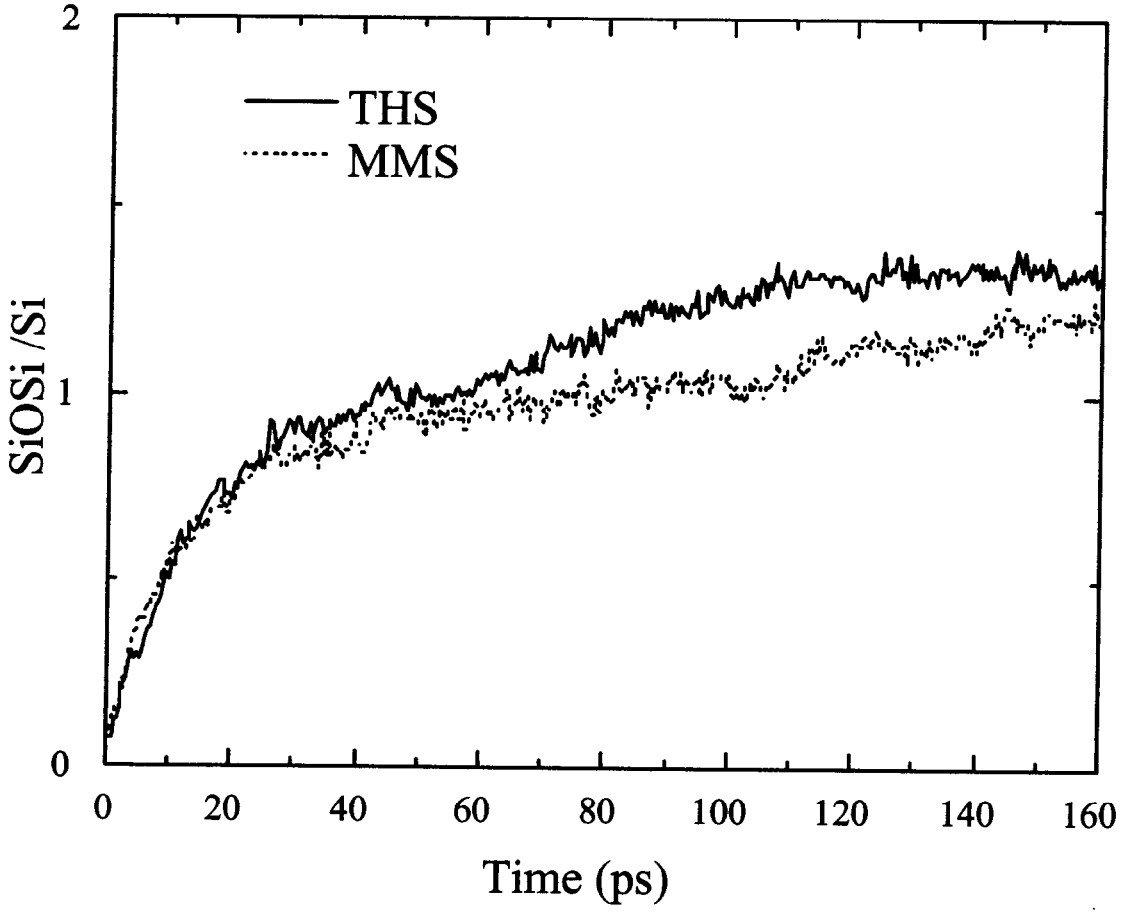

Fig. 4.2 Calculated SiOSi / Si ratio as a function of time.

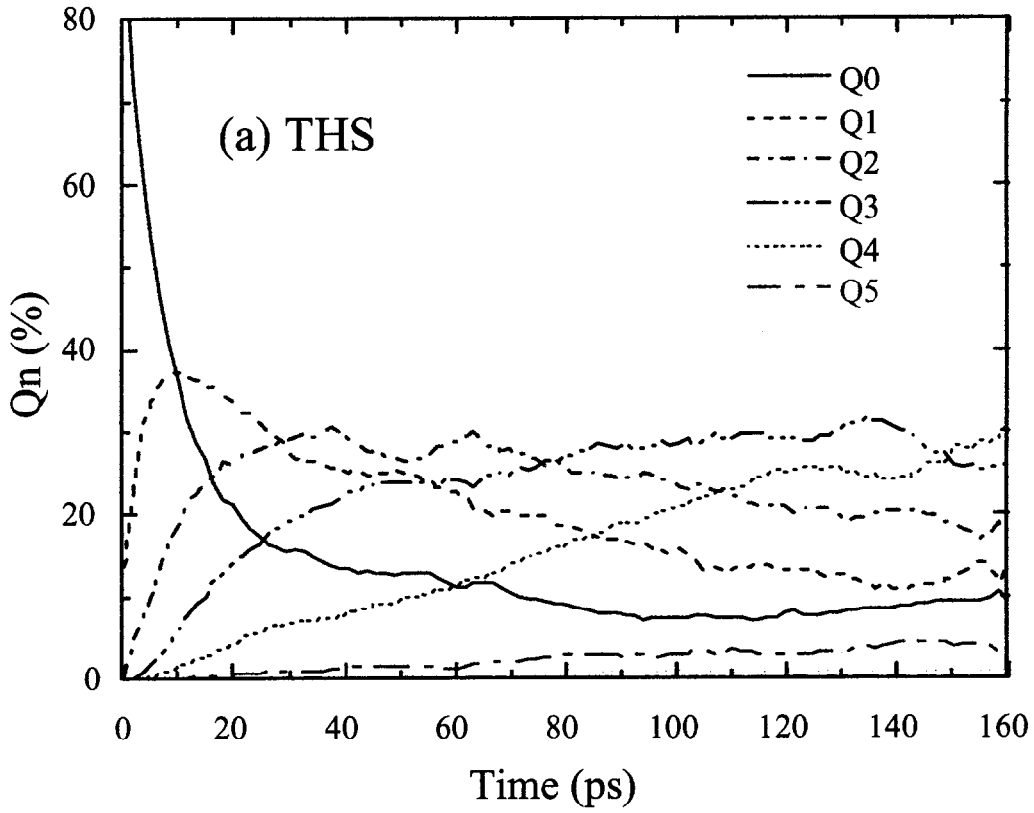

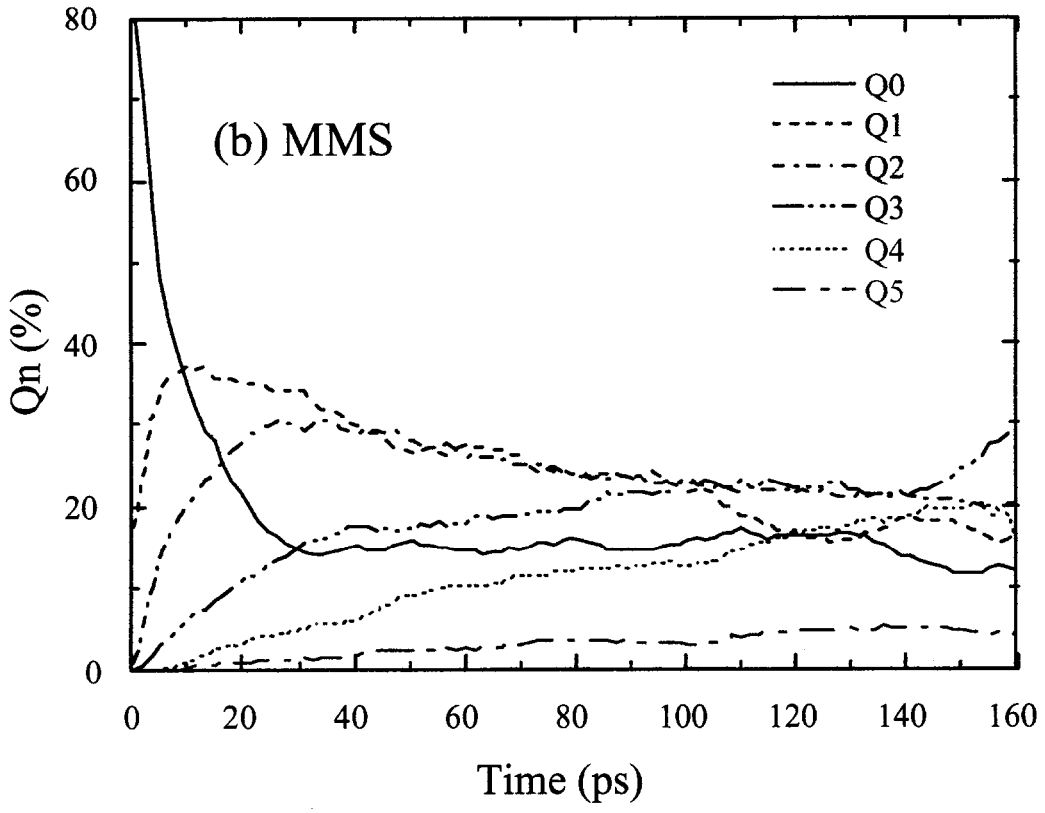

Fig. 4.3 Calculated composition of Q_n species as a function of time for THS (a, upper) and MMS (b, lower).

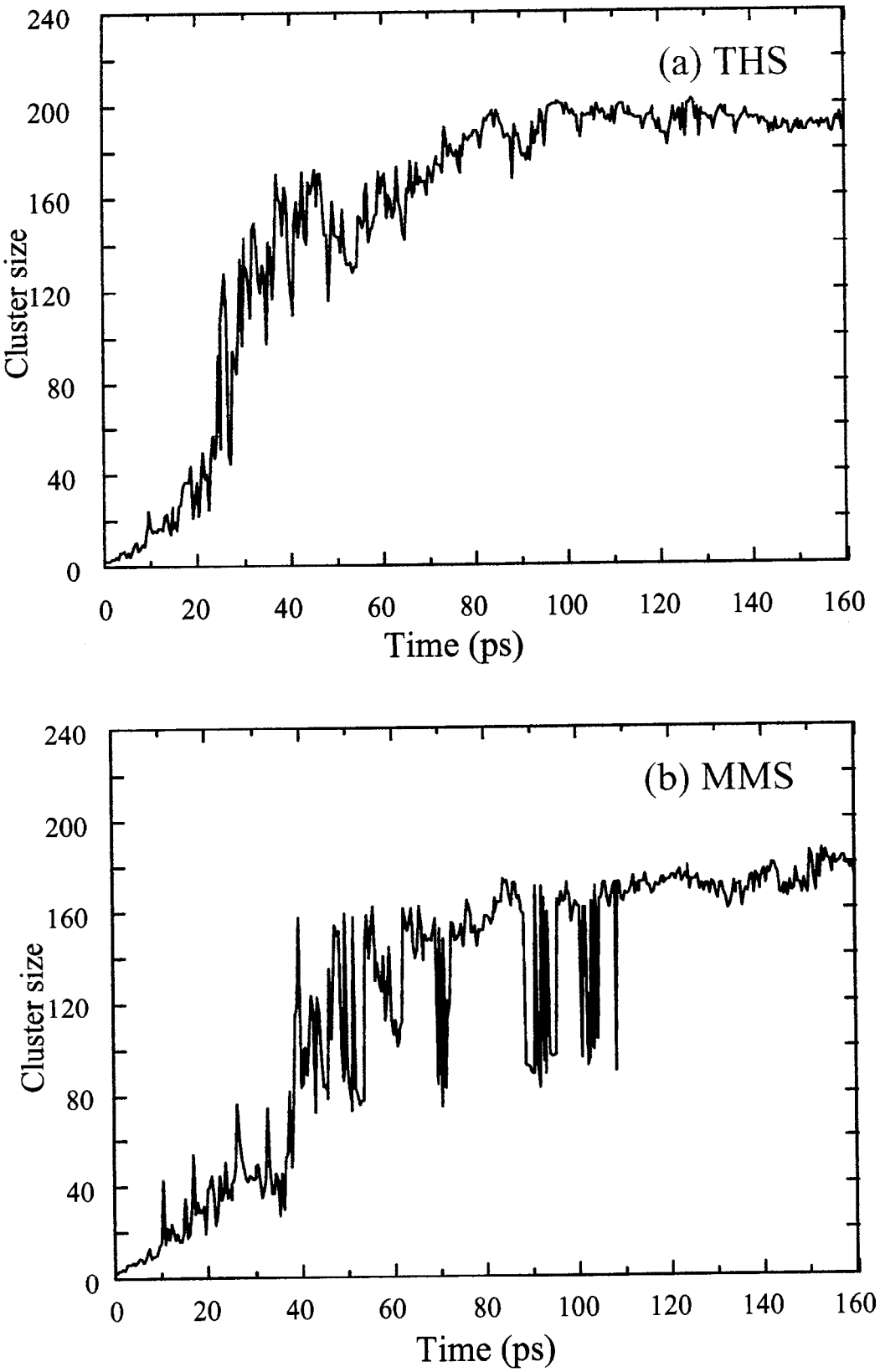

Fig. 4.4 Calculated maximum cluster size as a function of time for THS (a, upper) and MMS (b, lower).

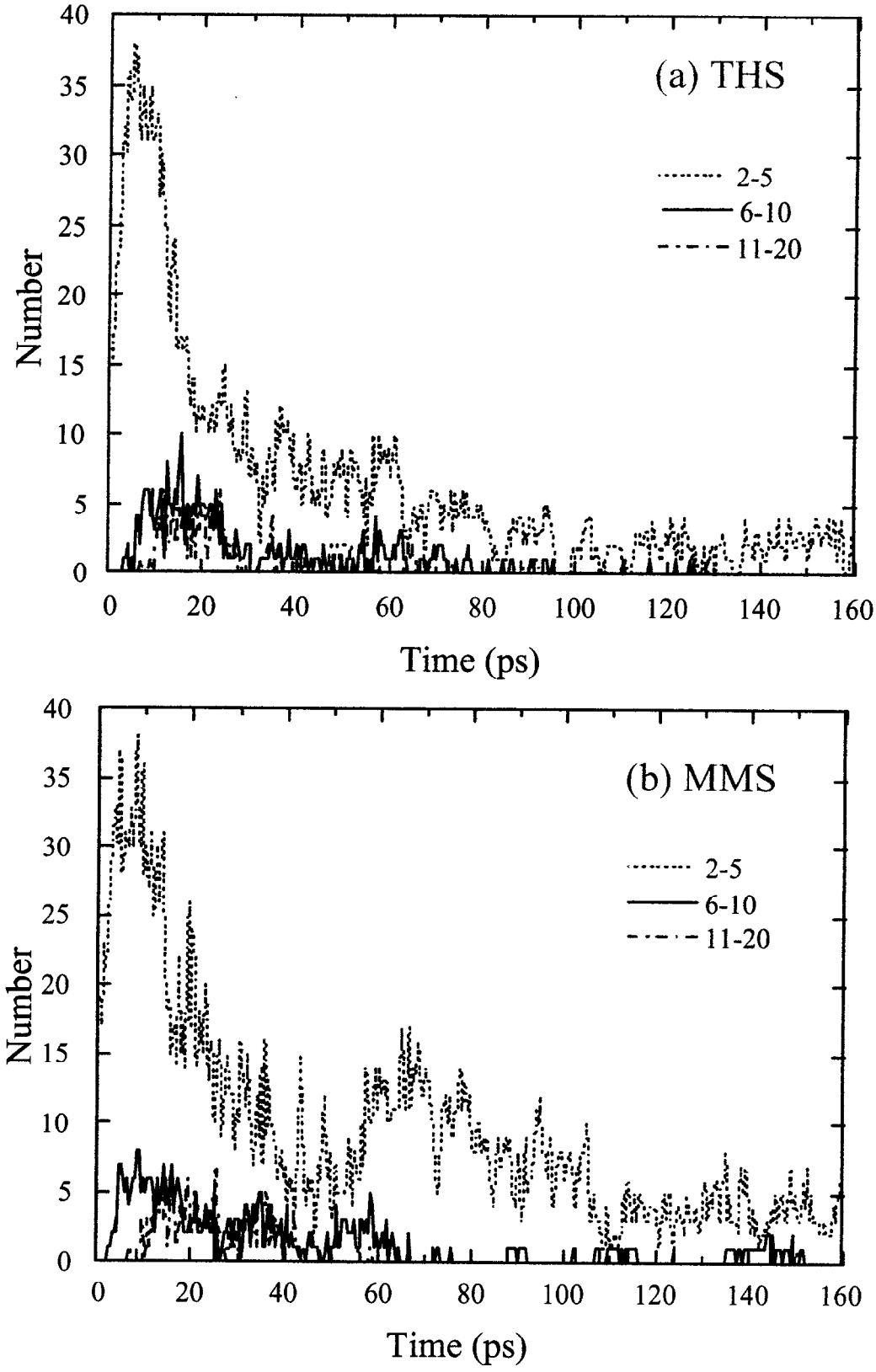

Fig. 4.5 Calculated number of small clusters as a function of time for THS (a, upper) and MMS (b, lower).

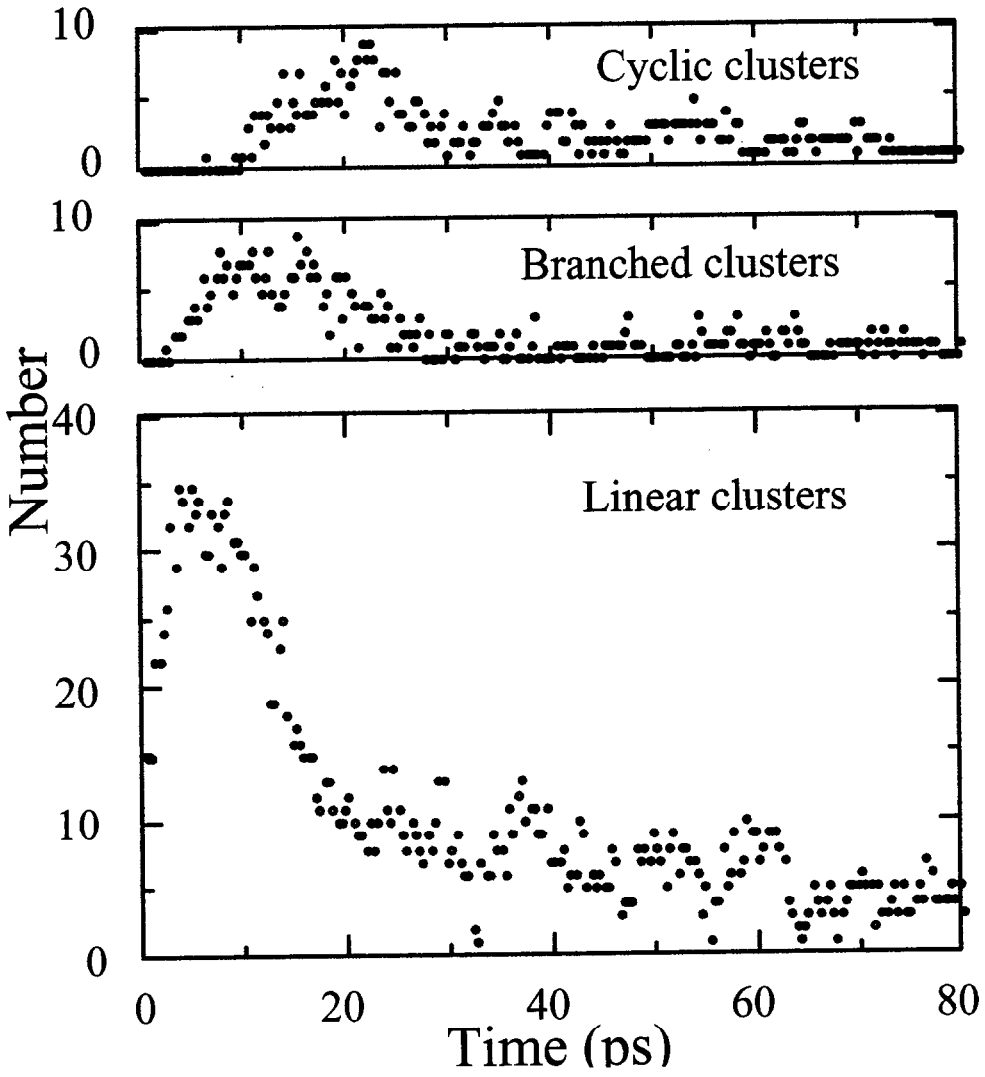

Fig. 4.6 Calculated number of each type of cluster as a function of time for THS.

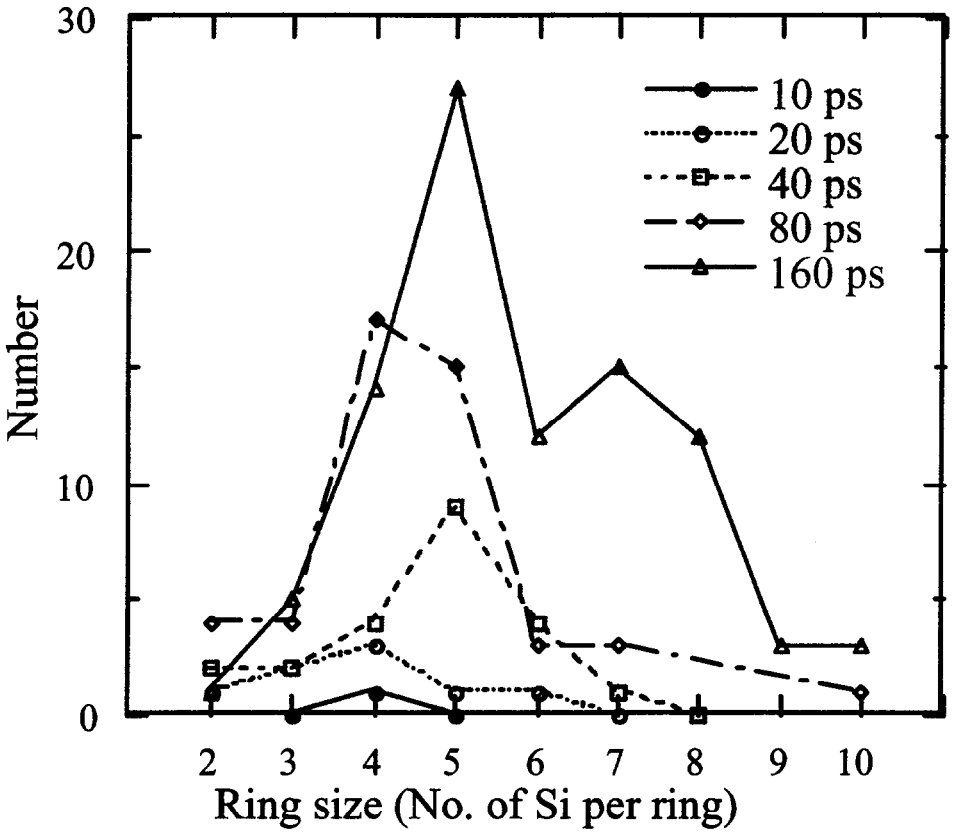

Fig. 4.7 Ring size distribution curves at different times for THS. The snapshots corresponding to the distribution are shown in Fig. 4.8.

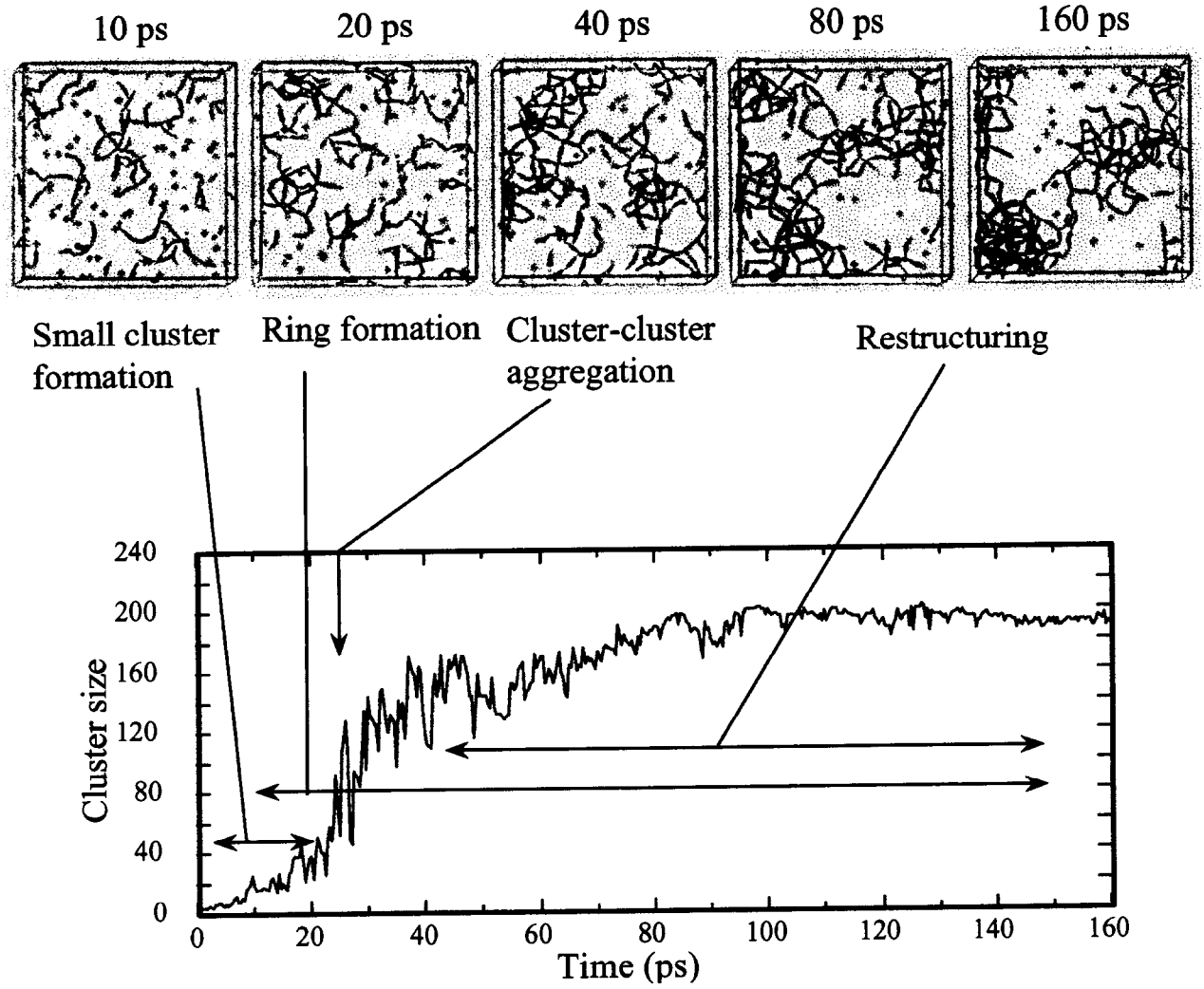

Fig. 4.8 Snapshots in the structural development for THS, with the maximum cluster size as a function of time given in Fig. 4.4 (a).

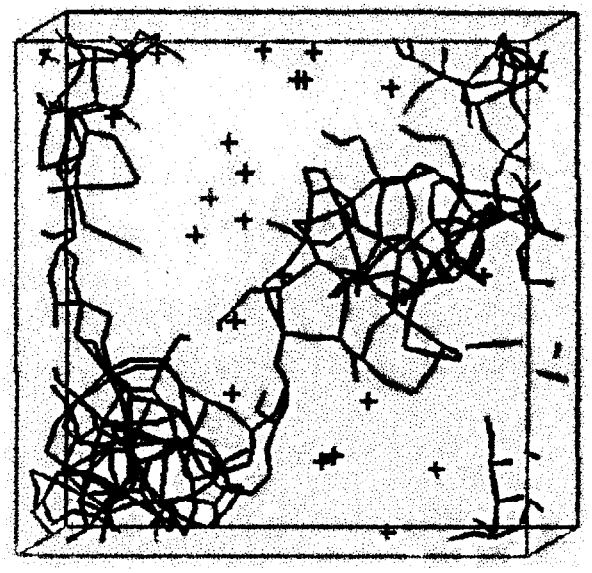

THS

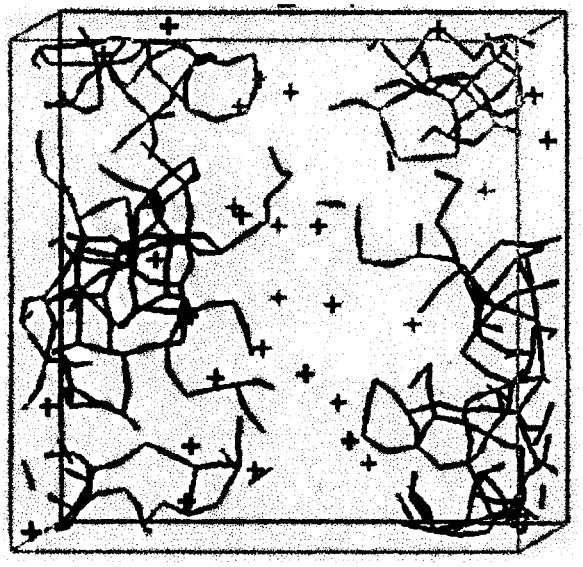

MMS

Fig. 4.9 Network structure for THS (upper) and MMS (lower) at 160 ps.

Chapter 5

Conclusion

MD simulations were applied to study thermal behaviour including displacive transitions and negative thermal expansions for cristobalite, an MFI-type zeolite, and silica glass/melt.

In chapter 2, the MD simulations reproduce the α-β phase transition of cristobalite, the negative thermal expansion of β-cristobalite, and the density anomaly of the silica melt. The thermal expansion of cristobalite is closely related to the distances between the nearest neighbor silicon atoms originating from the Si-O-Si angle. On the other hand, the thermal expansion of amorphous silica is governed by the longer-range structure i.e. the network-forming rings. Furthermore, the density anomaly of silica melt is caused by two opposite factors in the density variation with decreasing temperature: densification due to the increase in number of bridging bonds, and opening of the tetrahedral network due to the rearrangement of network-forming rings.

In chapter 3, the MD simulation of the MFI-type zeolite well reproduces the orthorhombic structure above the transition temperature and the monoclinic lattice below the transition temperature. The phase transition similar to the experimentally observed one takes place, and the vibrational spectra are also in reasonable agreement with the experimental ones. Thus the potential model used is sufficeintly appropriate for the MD simulations of this type of zeolite. In the MD simulations, the low-temperature monoclinic phase shows *Pn* symmetry instead of the experimentally reported $P2_1/n$ symmetry. In addition, a cooperative atomic displacement between two monoclinic *Pn* configurations is found at 250 K. The average structure of the two *Pn* configurations almost shows the $P2_1/n$ symmetry. Thus the MD simulations suggest the existence of monoclinic *Pn* phase as well as the experimental $P2_1/n$ phase. It is also found that the thermal expansion becomes negative in the higher temperature range (>500 K), similar to that observed for β-quartz and β-cristobalite. In the temperature range simulated, the thermal expansion of this zeolite almost corresponds to the variation in the Si-Si distance, and the very low thermal expansion is ascribed to the decrease in the Si-O-Si angle.

In chapter 4, polymerization process yielding gels was studied using MD simulations for silicic acid and monomethoxy silicic acid. The calculated Qn species distribution as a function of SiOSi/Si ratio is in good agreement with that observed by ^{1}H-NMR, suggesting the validity of the MD simulations. Atomistic features of the structural development were extracted from a series of the simulation results. There is a slow cluster growth during the early stage, a rapid cluster growth followed this due to cluster-cluster aggregation, and the network structure become denser with time through the repeated bond-formation and bond-breaking. Finally the tendency of phase separation is observed. The remaining methoxy group interferes with the aggregation and the formation of the dense network structure. The present simulation performed gives a reasonable picture from an atomistic point of view.

In conclusion, the present MD simulations qualitatively reproduce the experimental thermal behaviour such as the temperature induced displacive transitions of cristobalite and the MFI-type zeolite, and the negative thermal expansion of cristobalite and silica melt. Thus the MD simulations are widely effective not only for amorphous silica and known silica polymorphs but also for microporous crystals of zeolites. In addition, the complicated thermal expansion for the silica is successfully understood from an atomistic point of view as follows. The thermal expansion of crystalline silica is closely related to the distances between the nearest neighbor silicon atoms originating from the Si-O-Si bond angle. On the other hand, the thermal expansion of amorphous silica is dominated by longer-range structure such as network-forming rings. Furthermore, the MD simulations predict some thermal properties for the MFI-type zeolite that are a negative thermal expansion for the orthorhombic phase at higher temperatures, and the existence of a monoclinic *Pn* phase as well as the experimentally reported monoclinic $P2_1/n$ phase. Table 5.1 summarizes what the MD simulations reproduce and predict on the thermal behaviour of amorphous and crystalline silica, as well as the polymerization of silica systems.

It is desirable that those predictions by the MD simulations are confirmed experimentally. The next important applications of MD simulations are, for instance, the structures and dynamics of multi phase systems including grain boundaries. The performance of functional ceramics is mostly governed by the structures and properties of grain boundaries or surfaces as well as those of bulk. For the application of MD simulations to this field, the expansion of the scale of simulation systems and the introduction of some coarse-graining model would be necessary, as well as improving the accuracy of the present interatomic potential models.

Table 5.1 Reproduced properties and new insights from MD simulations.

	Reproduced	New insights
Amorphous silica	**Density anomaly**	**Network rings→thermal expansion** **Network opening→density anomaly**
Cristobalite	**Lattice shape** **α-β transition** **Negative thermal expansion**	**Si-O-Si→thermal expansion**
MFI zeolite	**Lattice parameters** **ORTHO-MONO transition**	**Si-O-Si→thermal expansion** ***P*2$_1$/*n* struct. is an ave. of two *Pn* config.** **The existence of *Pn* phase at lower T** **The existence of high temp. phase at T>500K**
Polymerization process	**Qn composition v.s. SiOSi/Si**	**Reasonable atomistic pictures** **Interference of methoxy gr. with gelation**

List of Publications

The original papers related to the present thesis are as follows.

1. K. Yamahara, K. Okazaki and K. Kawamura, "Molecular dynamics studies on thermal behaviour of an MFI-type zeolite", Catalysis Today, **23** (1995) 397.

2. K. Yamahara and K. Okazaki, "Molecular dynamics simulation of the structural development in sol-gel process for silica systems", Fluid Phase Equilibria, **144** (1998) 449.

3. K. Yamahara, K. Okazaki, K. Kawamura, "Molecular dynamics study of thermal behaviour of silica glass/melt and cristobalite", J. Non-Cryst. Solids, **291**, 1-2 (2001) 32.

The following papers are not directly related to the present thesis.

4. R. Takagi and K. Yamahara, "Structure of the molten $ZnCl_2$ near cathode", Mater. Trans., JIM, **33**, 10 (1992) 879.

5. T. Shoda, K. Yamahara, K. Okazaki and D.E. Williams, "Molecular packing analysis: prediction of experimental crystal strcutures of benzene starting from unreasonable initial structures" J. Mol. Struc., (Theochem), 313 (1994) 321.

6. T. Shoda, K. Yamahara, K. Okazaki and D.E. Williams, "Molecular packing analysis of benzene crystals. Part 2. Prediction of experimental crystal structure polymorphs at low and high pressure", J. Mol. Struc., (Theochem), 333 (1995) 267.

7. K. Saito, N. Ogawa, A.J. Ikushima, Y. Tsurita and K. Yamahara, "Effects of aluminum impurity on the structural relaxation in silica glass", J. Non-Cryst. Solids, **270** (2000) 60.

8. X. Huang, K. Yamahara and K. Hoshikawa, "In situ observation of the Si melt-silica glass interface concerning CZ-Si crystal growth", Mater. Sci & Eng. B **72** (2000) 164.

9. X. Huang, T. Wang, K. Yamahara, T. Taishi and K. Hoshikawa, "In situ observation of the interfacial phase formation at Si melt/silica glass interface", Jpn. J. Appl. Phys., 39 (2000) 3281.

10. K. Yamahara, X. Huang, S. Sakai, A. Utsunomiya, Y. Tsurita and K. Hoshikawa, "Surface of silica glass reacting with silicon melt: Effect of raw materials for silica crucibles", Jpn. J. Appl. Phys., **40** (2001) 1178.

11. K. Hoshikawa, X. Huang, S. Sakai, S. Oishi, T. Taishi and K. Yamahara, "Dynamic behaviour of oxygen, heavily doped other impurities and grown-in defect in the Czochralski Si crystal growth", Proceedings of the Fifth Symposium on Atomic-scale Surface and Interface Dynamics, March 1-2, 2001, Tokyo.

Acknowledgments

I can not express how grateful I am to Prof. Katsuyuki Kawamura (Tokyo Institute of Technology) for his guiding me in the molecular dynamics studies as well as for fruitful discussion and continuous encouragement throughout this study. I would like to express my sincere gratitude to Dr. Keiji Okazaki (Mitsubishi Chemical Corporation), who stimulated my interest in the molecular simulations of silica materials and gave me invaluable suggestions and continuous encouragement. Indeed, it was their guidance and cooperation that lead me to complete this thesis.

I would like to acknowledge my colleagues at Mitsubishi Chemical Corporation. Dr. Hisao Takeuchi and Dr. Takayuki Shoda for their in-depth discussion and encouragement. Dr. Yasushi Tsurita offered useful suggestions from an experimental point of view and encouragement. Dr. Kenichi Yoshie stimulated my interest in silica gel.

I wish to express my gratitude to Prof. Minoru Tomozawa (Rensselaer Polytechnic Institute) and Associate Prof. Kazuya Saito (Toyota Technological Institute) for invaluable discussion on the structures and dynamic properties of silica glass. I am grateful to Emeritus Prof. Tetsuo Takaishi (Toyohashi University of Technology) for stimulating my interest in the framework dynamics of zeolites in terms of their effects on catalytic action. I am also grateful to Prof. Stephen H. Garofalini (Rutgers University) for useful discussion on the MD study of polymerization yielding silica gel. I am deeply indebted to the late Prof. Ryuzo Takagi, who introduced me to MD simulations during the master's course, Tokyo Institute of Technology.

Finally, I would like to thank my parents, wife and sons for supporting and understanding me.